Faculty of Aerospace Engineering

Attitude Control of a Small Helicopter UAV

using Incremental Nonlinear Dynamic Inversion

B.J.M.M. Slinger

June 10, 2016

Delft University of Technology

Challenge the future

Attitude Control of a Small Helicopter UAV

using Incremental Nonlinear Dynamic Inversion

Master of Science Thesis

For obtaining the degree of Master of Science in Aerospace Engineering
at Delft University of Technology

B.J.M.M. Slinger

June 10, 2016

Faculty of Aerospace Engineering · Delft University of Technology

Delft University of Technology

Delft University Of Technology
Department Of
Control and Simulation

The undersigned hereby certify that they have read and recommend to the Faculty of Aerospace Engineering for acceptance a thesis entitled **"Attitude Control of a Small Helicopter UAV"** by **B.J.M.M. Slinger** in partial fulfillment of the requirements for the degree of **Master of Science**.

Dated: June 10, 2016

Readers:

Dr. ir. Q.P. Chu

Ir. B.D.W. Remes

Ir. E.J.J.Smeur

Dr.ir. E. van Kampen

Dr.ir. M. Voskuijl

Acronyms

AHRS	Attitude and Heading Reference System
DOF	Degrees Of Freedom
DSP	Digital Signal Processor
FPU	Floating Point Unit
INDI	Incremental Nonlinear Dynamic Inversion
MEMS	Micro-Electrical-Mechanical system
MIMO	Multiple Input Multiple Output
NDI	Nonlinear Dynamic Inversion
RPM	revolutions per minute
TPP	Tip-Path Plane
UAV	Unmanned Aerial Vehicle
VTOL	Vertical Takeoff and Landing

Contents

Acronyms v

I Research Paper 1

II Additional Work 17

1 Attitude Estimation 19
- 1-1 Fusion algorithms 19
- 1-2 Explicit Complementary Filter 20
- 1-3 Vibrations 21
- 1-4 Accelerations 21
- 1-5 Performance Evaluation 21

2 INDI Derivations 25
- 2-1 Closed Loop Input Tracking 25
- 2-2 Control Effectiveness Mismatch 26
- 2-3 Disturbance Rejection 27
- 2-4 Actuator Model Mismatch 28

III Literature Study 31

3 Introduction 33
- 3-1 Research questions 34
  - 3-1-1 Attitude estimation 34
  - 3-1-2 Helicopter INDI control 35
- 3-2 Layout 35

4 Test Equipment **37**
4-1 Helicopter . . . 37
4-2 Brushless upgrade . . . 37
4-3 Autopilot . . . 39
4-4 MEMS gyroscopes and accelerometers . . . 40
4-4-1 Accelerometer measurements . . . 40
4-4-2 Gyroscope measurements . . . 40
4-4-3 Amplitude and frequency limitations . . . 40
4-4-4 Thermal MEMS accelerometers . . . 41

5 Attitude Estimation **43**
5-1 Basic concept . . . 43
5-2 Kalman filter . . . 44
5-2-1 Linear Kalman filter . . . 44
5-2-2 Attitude representations . . . 44
5-2-3 Direct and Indirect Kalman filter . . . 45
5-2-4 External accelerations . . . 45
5-3 Complementary filter . . . 46
5-3-1 Basic complementary filter . . . 46
5-3-2 Direct and passive complementary filter . . . 48
5-3-3 Explicit complementary filter . . . 50
5-3-4 External accelerations . . . 50
5-4 Vibration attenuation methods . . . 51
5-4-1 Mechanical damping . . . 51
5-4-2 Software filtering . . . 51

6 Helicopter Dynamics and Control **53**
6-1 Helicopter Model . . . 53
6-2 Rotor types . . . 54
6-2-1 Teetering rotor . . . 54
6-2-2 Fully articulated rotor . . . 54
6-2-3 Hingeless rotor . . . 55
6-3 Dynamics of a spinning disc . . . 56
6-4 Control . . . 57
6-4-1 PID control . . . 57
6-4-2 Other control methods . . . 58

7 Incremental Nonlinear Dynamic Inversion for Helicopter Control 59
7-1 Motivation 59
7-2 Nonlinear Dynamic Inversion 60
7-3 Incremental Nonlinear Dynamic Inversion 61
7-3-1 Actuator dynamics 61
7-3-2 Disturbance rejection 63
7-3-3 Output measurement filtering 63
7-4 INDI for helicopter rate control 64
7-4-1 Incremental rate control loop 64
7-4-2 Simulation 67

8 Project Planning 69
8-1 Attitude estimation 69
8-2 INDI controller implementation 70

9 Conclusions 71
9-1 Attitude estimation 71
9-2 Helicopter INDI control 71

Bibliography 73

Part I

Research Paper

Discrete Incremental Nonlinear Dynamic Inversion for Attitude Control of a Small Helicopter UAV

B.J.M.M. Slinger[a,*], E.J.J. Smeur[a], Q.P. Chu[a], B.D.W. Remes[a]

[a] *Delft University of Technology, Delft, Zuid-Holland, 2629HS, Netherlands*

Abstract

This paper presents an attitude controller for a small helicopter Unmanned Aerial Vehicle (UAV) based on Incremental Nonlinear Dynamic Inversion (INDI). INDI is a sensor-based control method which responds quickly to the commanded input, but also to disturbances. While previous implementations of INDI used a control effectiveness matrix describing effects on rotational *accelerations*, the implementation presented in this paper uses rotational *rates*. This is possible with small hingeless-rotor helicopters since the rotational rates are achieved almost immediately, but also the transient is taken into account. By doing so, the matrix contains only constants and the control structure is much simpler. The proposed controller is implemented on a small helicopter which weighs less than 50 grams. The performance of the controller is demonstrated with step responses on roll and heading angles. Also disturbance rejection capabilities are demonstrated. Finally, the controller is deliberately configured incorrectly with wrong control effectiveness and actuator model parameters. A theoretical derivation is provided to predict the effect of incorrect parameters. With experiments, it is demonstrated that the helicopter can be stabilized over a wide range of incorrect values. It is concluded that the demonstrated controller is a suitable choice for small autonomous helicopters.

1. Introduction

The multi-rotor configuration is the most common type of Unmanned Aerial Vehicle (UAV) nowadays. The design is mechanically simple and robust, since the motors are the only moving parts. The maneuverability is generally very good. With a properly tuned attitude controller it is also relatively easy to fly. The downside of the multi-rotor concept is its lower efficiency. A set of smaller rotors is less efficient than a single large rotor that delivers the same amount of thrust [1]. This is exactly what the classical helicopter is. Even with a tail-rotor to compensate for torque of the main rotor, it is more energy efficient. This energy efficiency is a trade-off with robustness. The mechanical design of a helicopter is more complex with servo actuators and a swash-plate mechanism. The design of an attitude controller is more complicated because several cross-coupling effects have to be taken into account.

Prox Dynamics has developed the PD-100 Black Hornet, which is a miniature helicopter for military applications, but no details are available on its capabilities and inner workings. In literature, a lot of work can be found on autonomous helicopters, although these helicopters are much larger. PID control is a common attitude control strategy in literature [2, 3]. Other control strategies include input/output linearization [4], gain scheduling [5], LQR control [6, 7], neural networks [8, 9] and reinforcement learning [10].

Figure 1: Walkera Genius CP V2 unmodified.

In this paper, an attitude controller is designed for a small helicopter UAV (Fig. 1), weighing only 45 grams. To be able to fly in windy conditions in an urban environment, it is necessary to quickly counteract any disturbances. Incremental Nonlinear Dynamic Inversion (INDI) [11] is a sensor-based control method which has good disturbance rejection qualities [12]. Using sensor measurements, the system is feedback linearized and a simple linear controller can be added to control the attitude. Once the control effectiveness in the INDI loop has been identified, which can be done automatically by an adaptive algorithm, the UAV shows excellent flight characteristics. This technique was recently implemented on quadcopters with impressive results [12]. However, the same controller cannot be used directly on helicopters.

Simplicio et al. [13] demonstrated the use of INDI already on a full size helicopter in a simulation study. The control effectiveness functions for helicopters are much more complicated, which significantly reduces the simplicity of

*Corresponding author

the controller. In fact, the most complicated part of the helicopter dynamics are contained in the control effectiveness functions. These functions describe the relations between control inputs and angular *accelerations*. For quadcopters, the actuator effectiveness with respect to angular accelerations can be approximated by a matrix with constants. This is impossible for helicopters since the actuator effectiveness with respect to angular accelerations is actually a function of rotational rates and more.

To reduce the complexity while maintaining the robustness, a method is proposed which implements INDI in a different way. Instead of looking for a relation between actuator deflections and rotational accelerations, a relationship is found with steady-state rotational *rates*. The damping dynamics in roll and pitch are very fast, so these steady-state rates are reached almost immediatly. The actuator effectiveness in pitch and roll can then be described by constants, which can be identified in flight.

Section 2 shows the derivation of the closed-loop response of INDI. Also the system response in case of disturbances and modelling errors are provided. Section 3 describes the new control structure for helicopters in detail. In Section 4, the hardware is described which was used to test the new controller implementation, including models of the actuators. The control effectiveness experiments and calculations are provided in Section 5. Section 6 provides the results and discussions of various experiments to evaluate the performance of the new controller. The paper concludes with conclusions and recommendations in Section 7.

2. Incremental Nonlinear Dynamic Inversion

Until now, INDI is always derived from a continuous-time system. This derivation of the control law is shown in Section 2.1. In Section 2.2, a discret control law is derived from a discretized linearized system. Real systems usually have actuators, which are added in Section 2.3. The addition of a measurement filter is shown in Section 2.4. The disturbance rejection characteristics are derived in Section 2.5. Section 2.6 and 2.7 show the effect of errors in the control effectiveness and actuator model.

2.1. Continuous-time INDI

Previous publications on INDI [11, 13, 12] start the derivation of the control law from a continuous-time system:

$$\dot{\mathbf{x}} = f(\mathbf{x}, \mathbf{u}) \tag{1}$$

It is assumed that all states of the system are measurable. This system is then linearized around $\mathbf{x}_0, \mathbf{u}_0$, which gives:

$$\begin{aligned}\dot{\mathbf{x}} \approx f(\mathbf{x}_0, \mathbf{u}_0) &+ \left.\frac{\partial f(\mathbf{x}, \mathbf{u})}{\partial \mathbf{x}}\right|_{\mathbf{x}_0, \mathbf{u}_0} (\mathbf{x} - \mathbf{x}_0) \\ &+ \left.\frac{\partial f(\mathbf{x}, \mathbf{u})}{\partial \mathbf{u}}\right|_{\mathbf{x}_0, \mathbf{u}_0} (\mathbf{u} - \mathbf{u}_0)\end{aligned} \tag{2}$$

This can be written as follows:

$$\dot{\mathbf{x}} \approx \dot{\mathbf{x}}_0 + \mathbf{F}(\mathbf{x}_0, \mathbf{u}_0)\Delta\mathbf{x} + \mathbf{G}(\mathbf{x}_0, \mathbf{u}_0)\Delta\mathbf{u} \tag{3}$$

It is assumed that $\dot{\mathbf{x}}_0$ can be measured. The term related to system dynamics $\mathbf{F}$ is assumed to be much smaller than the term related to the increment in control input. This principle is often referred to as time-scale separation [13]. By neglecting this term, the equation is reduced to:

$$\dot{\mathbf{x}} \approx \dot{\mathbf{x}}_0 + \mathbf{G}(\mathbf{x}_0, \mathbf{u}_0)\Delta\mathbf{u} \tag{4}$$

The control law is obtained by inverting the equation:

$$\Delta\mathbf{u} = \mathbf{G}^{-1}(\mathbf{x}_0, \mathbf{u}_0)\left[\boldsymbol{\nu} - \dot{\mathbf{x}}_0\right] \tag{5}$$

Where $\boldsymbol{\nu}$ is the virtual control input and $\dot{\mathbf{x}}_0$ is the measurement of the current state derivative. By applying this control law to Eq. 4, the response of the system becomes:

$$\dot{\mathbf{x}} = \boldsymbol{\nu} \tag{6}$$

2.2. Discrete-time INDI

The derivation of the control law for a discrete-time system starts with the discrete system:

$$\begin{aligned}\mathbf{x}_{k+1} &= \mathbf{x}_k + \int_0^{\Delta t} \dot{\mathbf{x}}\,\mathrm{d}t &(7)\\ &= \mathbf{x}_k + \int_0^{\Delta t} f(\mathbf{x}, \mathbf{u})\,\mathrm{d}t &(8)\end{aligned}$$

When the sample-rate is high, it can be assumed that $\dot{\mathbf{x}}$ remains constant for a period of Δt:

$$\mathbf{x}_{k+1} \approx \mathbf{x}_k + f(\mathbf{x}_k, \mathbf{u}_k)\,\Delta t \tag{9}$$

$$\frac{\mathbf{x}_{k+1} - \mathbf{x}_k}{\Delta t} \approx f(\mathbf{x}_k, \mathbf{u}_k) \tag{10}$$

The term on the right-hand side can be linearized with a first-order Taylor expansion around $\mathbf{x}_{k-1}, \mathbf{u}_{k-1}$:

$$\begin{aligned}\frac{\mathbf{x}_{k+1} - \mathbf{x}_k}{\Delta t} &\approx f(\mathbf{x}_{k-1}, \mathbf{u}_{k-1}) \\ &+ \left.\frac{\partial f(\mathbf{x}_k, \mathbf{u}_k)}{\partial \mathbf{x}_k}\right|_{\mathbf{x}_{k-1}, \mathbf{u}_{k-1}} (\mathbf{x}_k - \mathbf{x}_{k-1}) \\ &+ \left.\frac{\partial f(\mathbf{x}_k, \mathbf{u}_k)}{\partial \mathbf{u}_k}\right|_{\mathbf{x}_{k-1}, \mathbf{u}_{k-1}} (\mathbf{u}_k - \mathbf{u}_{k-1})\end{aligned} \tag{11}$$

which can be written as:

$$\begin{aligned}\frac{\mathbf{x}_{k+1} - \mathbf{x}_k}{\Delta t} = f(\mathbf{x}_{k-1}, \mathbf{u}_{k-1}) &+ \mathbf{F}(\mathbf{x}_{k-1}, \mathbf{u}_{k-1})\Delta\mathbf{x}_k \\ &+ \mathbf{G}(\mathbf{x}_{k-1}, \mathbf{u}_{k-1})\Delta\mathbf{u}_k\end{aligned} \tag{12}$$

By substituting Eq. 10 for $\mathbf{x}_{k-1}, \mathbf{u}_{k-1}$ and by applying the principle of time-scale separation [13], the equation is reduced to:

$$\frac{\mathbf{x}_{k+1} - \mathbf{x}_k}{\Delta t} = \frac{\mathbf{x}_k - \mathbf{x}_{k-1}}{\Delta t} + \mathbf{G}(\mathbf{x}_{k-1}, \mathbf{u}_{k-1})\Delta\mathbf{u}_k \tag{13}$$

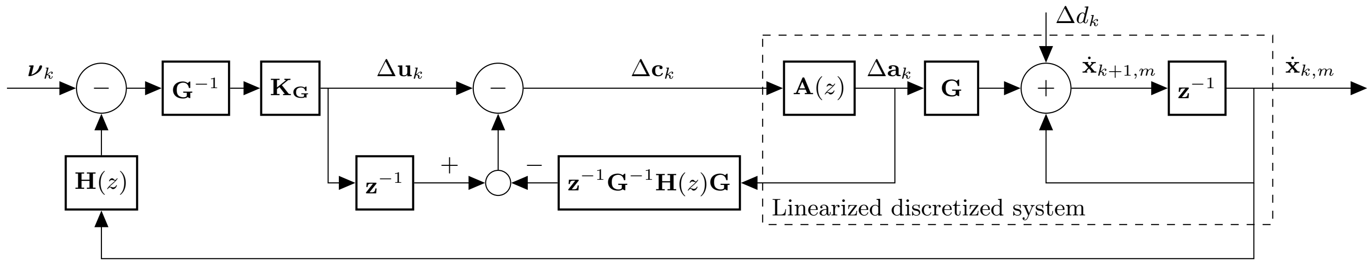

Figure 2: INDI block diagram for a discretized linearized system actuator dynamics $\mathbf{A}(z)$, a measurement filter $\mathbf{H}(z)$, a control effectiveness $\mathbf{G}$ and control effectiveness error scalar $\mathbf{K}_G$.

This equation can be inverted to get the control law:

$$\Delta\mathbf{u}_k = \mathbf{G}^{-1}(\mathbf{x}_{k-1}, \mathbf{u}_{k-1})\left[\boldsymbol{\nu}_k - \dot{\mathbf{x}}_{k,m}\right] \tag{14}$$

where

$$\dot{\mathbf{x}}_{k,m} = \frac{\mathbf{x}_k - \mathbf{x}_{k-1}}{\Delta t} \tag{15}$$

$$\boldsymbol{\nu}_k = \frac{\mathbf{x}_{k+1} - \mathbf{x}_k}{\Delta t} \tag{16}$$

$\dot{\mathbf{x}}_{k,m}$ is obtained from the measurement of the state $\mathbf{x}_k$ and $\boldsymbol{\nu}_k$ is the virtual control. The result is very similar to the continuous case, but now with a discrete approximation of the state derivative.

2.3. Actuator Dynamics

The theoretical derivation of the control law assumes that the requested actuator deflection is obtained immediately. Real systems are usually limited by the dynamics of the actuators. Because of the actuator dynamics, a change in the actuator command does not immediately result in the desired system output. The actuator basically delays the command. The control law will keep commanding more increments while the output has not reached the target, because it is unaware of the actuator dynamics.

A modification of the command law is required such that it takes into account the movement of the actuator that is still to come. $\Delta\mathbf{a}_k$ represents the actual change in actuator deflections, which is assumed to be measurable. $\Delta\mathbf{c}_k$ is the commanded increment to the actuator, which contains the correction term:

$$\Delta\mathbf{c}_k = \Delta\mathbf{u}_k - (\Delta\mathbf{u}_{k-1} - \Delta\mathbf{a}_{k-1}) \tag{17}$$

The corresponding block diagram is shown in Fig. 2. The transfer function of this block diagram is given by:

$$\dot{\mathbf{x}}_m = \mathbf{z}^{-1}\mathbf{G}\mathbf{A}(z)\mathbf{G}^{-1}\boldsymbol{\nu} \tag{18}$$

This equation states that the system follows the virtual control, but is delayed by the actuator dynamics.

2.4. Measurement Filter

In practical applications, an accurate measurement of the output variables is often not available. Sensor readings may have to be differentiated to obtain the output, which adds noise. Without a measurement filter, the INDI controller will also react to the noise.

By simply adding a measurement filter $\mathbf{H}(z)$ to the output, the closed loop dynamics would also change. However, if the filter is also applied in the actuator feedback loop, the open loop dynamics remain unchanged. This approach is similar to what was found in literature [14, 12]. The complete block diagram in Fig. 2 shows the INDI control loop with the measurement filters $\mathbf{H}(z)$ in place. The system response is exactly the same as in Eq. 18. However, the addition of a measurement filter reduces disturbance rejection as is shown in Section 2.5.

2.5. Disturbance Rejection

A disturbance is added to the output of the system, such that

$$\dot{\mathbf{x}}_{k+1,m} = \dot{\mathbf{x}}_{k,m} + \mathbf{G}\Delta\mathbf{a}_k + \Delta\mathbf{d}_k \tag{19}$$

Taking into account that $\Delta\mathbf{d}_k = \mathbf{d}_k - \mathbf{d}_{k-1}$, it can be shown that the output in response to a disturbance is given by:

$$\dot{\mathbf{x}}_m = \mathbf{z}^{-1}\left[\mathbf{I} - \mathbf{z}^{-1}\mathbf{G}\mathbf{A}(z)\mathbf{G}^{-1}\mathbf{H}(z)\right]\mathbf{d}_k \tag{20}$$

This equation shows that the disturbances are damped out. The damping dynamics consists of the actuator dynamics and the measurement filter dynamics. The faster these dynamics are, the faster the disturbance is rejected.

2.6. Control Effectiveness Mismatch

Inaccuracies in the control effectiveness matrix $\mathbf{G}$ do not cause steady-state errors because of the incremental nature of INDI. It will however change the closed loop dynamics. If the effectiveness matrix is overestimated, the inverse will be smaller resulting in a smaller control increment. On the other hand, if the effectiveness matrix is underestimated, the control increment becomes larger. The inaccuracies are modeled as a gain $\mathbf{K}_G$, which results in the following modified control law:

$$\Delta\mathbf{u}_k = \mathbf{K}_G\mathbf{G}^{-1}\left[\boldsymbol{\nu}_k - \mathbf{H}(z)\dot{\mathbf{x}}_{k,m}\right] \tag{21}$$

A $\mathbf{K}_G$ with values lower than one corresponds to an overestimated control effectiveness matrix. The smaller $\mathbf{K}_G$ becomes, the slower the system tracks the virtual control.

A $\mathbf{K}_G$ with values larger than one corresponds to an under-estimated control effectiveness matrix.

For a single degree of freedom, with no measurement filter, the closed-loop transfer function is:

$$\dot{x}_m = \frac{A(z)K_G}{z + A(z)(K_G - 1)}\nu \tag{22}$$

In case of no actuator dynamics, the system reduces to:

$$\dot{x}_m = \frac{K_G}{z + K_G - 1}\nu \tag{23}$$

This transfer function has one pole which is located at $p = (1 - K_G)$. For $0 \leq K_G \leq 2$, the pole resides within the unit-circle on the real axis, which means that the system is stable. A similar analysis is possible with actuator dynamics included. For example, if the actuator dynamics are first-order:

$$\Delta a_k = (1 - \beta)\Delta a_{k-1} + \beta \Delta u_k \tag{24}$$

with $0 < \beta \leq 1$. It has the following transfer function:

$$A(z) = \frac{z\beta}{z - 1 + \beta} \tag{25}$$

For this actuator, it can be shown that the closed-loop transfer function of the INDI-loop is given by:

$$\dot{x}_m = \frac{\beta K_G}{z + \beta K_G - 1}\nu \tag{26}$$

The result is very similar to Eq. 23, but now the closed-loop system response is stable for $0 \leq \beta K_G \leq 2$. The slower the actuator is, the lower β is, which results in a larger error margin for the control effectiveness matrix. Still, the correct sign in K_G is crucial for stability.

2.7. Actuator Model Mismatch

The INDI controller needs the output of the actuator dynamics in the inner feedback loop. In practical situations, the actuator deflections $\Delta \mathbf{a}_k$ cannot always be measured. In that case, a model has to be used. Errors in the model affect the open- and closed loop dynamics. An analysis is done for an actuator with first-order dynamics in a single degree of freedom. The actuator dynamics are given by Eq. 25. The actuator model is also a first order system, whose dynamics are described by:

$$M(z) = \frac{zK_A\beta}{z - 1 + K_A\beta} \tag{27}$$

in which the factor K_A describes the error in β with respect to the real actuator dynamics. The two extremes are $K_A = 0$ and $K_A = 1/\beta$. The first case results in a model with an output of zero. The latter case represents a model with direct feed-through of the input.

The block diagram of the control structure which uses the actuator model is shown in Fig. 3. It can be shown that the closed-loop response of the INDI-loop is then given by:

$$\dot{x}_m = \frac{A(z)}{z - M(z) + A(z)}\nu \tag{28}$$

which can be expanded to:

$$\dot{x}_m = \frac{z\beta - \beta + K_A\beta^2}{z^2 + z(2\beta - 2) + 1 - 2\beta + K_A\beta^2}\nu \tag{29}$$

The two poles of this second-order system can be found at:

$$p = \pm\sqrt{\beta^2 - K_A\beta^2} - \beta + 1 \tag{30}$$

The poles always stay within the unit circle when $0 \leq K_A \leq 1/\beta$. From $K_A > 1$, the poles have an imaginary part, which means that the system contains oscillations. To prevent oscillations, it is therefore preferred to estimate the actuator model to be slower than the actual actuator.

3. Attitude Control of a Small Helicopter UAV

This section describes the application of INDI control techniques to a small helicopter UAV. Previous work by Simplicio et al. [13] already implemented INDI in a simulation study for a Bölkow Bö-105 helicopter. This paper presents a far more simple implementation of INDI, by controlling directly roll and pitch *rates* instead of *accelerations* inside the INDI loop.

3.1. Pitch and Roll Control

The dynamics and coupling in the pitch and roll motion make it difficult to apply INDI in the same way as it was applied to quadcopters in [12]. In quadcopter control, the actuators generate forces which results in rotational accelerations. The deflection of the cyclic of a helicopter can also be directly related to angular accelerations, but there is also strong damping which causes the rotational rate to reach a steady-state value quickly. The traditional approach with INDI neglects the model dynamics, which includes this strong damping of rotational rates.

Simplicio et al. [13] implemented an INDI controller for a helicopter in a simulation study. The control effectiveness matrix describes the relation between control inputs and rotational *accelerations*. These relations cannot be described by a matrix with constant values. Instead, the control effectiveness matrix is the Jacobian matrix of the control effectiveness functions, which follows from the first-order Taylor expansion.

This method significantly reduces the simplicity of INDI, since the control effectiveness functions contain the most complicated part of the helicopter model. A new approach is introduced here. Instead of controlling the rotational accelerations, the rotational *rates* are selected as the control variables in INDI. A direct and affine relationship can be

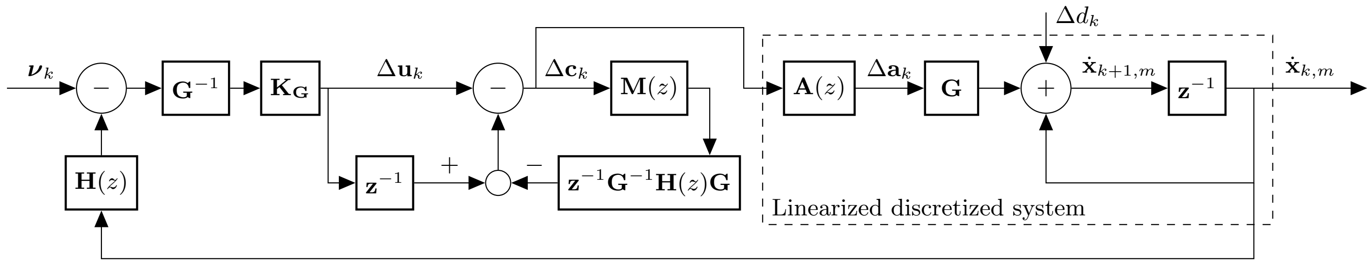

Figure 3: INDI block diagram for a discretized linearized system actuator dynamics $\mathbf{A}(z)$, an actuator model $\mathbf{M}(z)$, a measurement filter $\mathbf{H}(z)$, a control effectiveness $\mathbf{G}$ and control effectiveness error scalar $\mathbf{K}_G$.

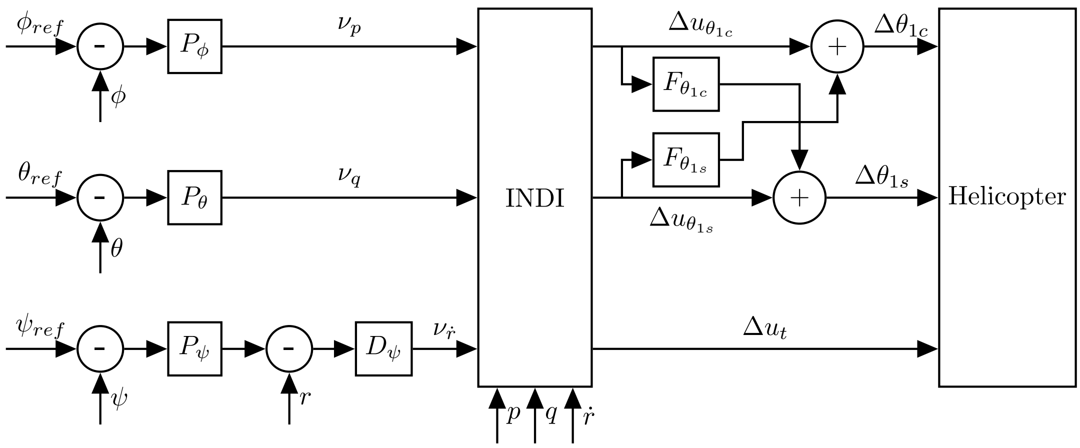

Figure 4: Helicopter attitude control loop.

obtained between the control inputs and *steady-state* rotational rates in pitch and roll. These constants go into the $\mathbf{G}$ matrix and are usable for a large section of the flight envelope. The rotational rate dynamics are not neglected, but accounted for in the same way as the actuator dynamics.

Since the INDI loop follows a rotational rate reference, only a proportional gain is required for stabilization of pitch and roll angles. Figure. 4 shows that the virtual control for pitch and roll is generated with a P-controller.

3.1.1. Fast Damping Dynamics

The actuator dynamics, as described in Section 2.3, are fast dynamics with a steady-state value of one. It could also be seen as a part of something more generic. The system $\mathbf{A}(z)$ can be described as fast dynamics of which the state is not controlled directly, but the steady-state value is.

In case of an actuator, the requested steady-state value is commanded and the actuator moves towards that position with certain dynamics. No effort is made by the INDI loop to increase the speed at which the actuators reaches this position. The actuator output $\mathbf{a}_k$ represents the actual position.

The fast damping dynamics of the rotational rates in pitch and roll can be implemented in the same way as the actuator dynamics. The dynamics of the rotational rates are already very fast, especially in the case of a hingeless rotor and little body inertia. The rate damping dynamics together with the actuator dynamics is represented by $\mathbf{A}(z)$. Implementing the rate damping like this basically means that the INDI controller accepts the delay caused by the rate damping dynamics. It is not possible to measure the state of the damping, so a simple first-order model needs to be used for that.

3.1.2. Pitch and Roll Coupling

The coupling between pitch and roll motion depends on the type of rotor. With a teetering rotor, there is no hub moment and rotational accelerations are generated only by tilting the rotor disc. The rotor disc is tilted by applying maximum blade pitch exactly 90° in advance. In this case, a lateral cyclic input will simply result in a roll acceleration.

With the articulated and hingeless rotor types, the pitch and roll dynamics are strongly coupled. A roll rate causes an additional pitch acceleration and a pitch rate causes an additional roll acceleration. The implementation of INDI by Simplicio et al. [13] actually accounts for these couplings because the control effectiveness functions include the pitch- and roll rate.

The approach taken here is very similar to what pilots do when flying a helicopter. Instead of steering towards the desired direction, the command is rotated to compensate a large portion of the couplings. A pitch command results in a very strong coupled roll acceleration. A roll command results in a relatively smaller coupling in pitch acceleration. The difference is caused by the differences in inertia around the roll and pitch axis. Therefore, different compensation factors apply to pitch and roll commands.

The corrections are not included in the control effectiveness matrix $\mathbf{G}$. Instead, the corrections are applied after the INDI controller, as shown in Fig. 4. This is effectively the same, but keeping $\mathbf{G}$ diagonal is more convenient. The compensation factors $F_{\theta_{1c}}$ and $F_{\theta_{1s}}$ are initially set to zero, which results in a flyable helicopter with small oscillations in pitch and roll. The factors can be tuned to reduce the couplings to a minimum.

3.2. Yaw Control

Acceleration in yaw is the result of moments generated by the tail rotor and main rotor. The tail rotor moment is approximated as a linear relation with the control input. The control input can either be tail rotor pitch or revolutions per minute (RPM), depending on the type of helicopter. The collective pitch is used to control vertical acceleration, but also generates a yaw moment with the rotor blade drag.

The tail rotor input controls yaw acceleration while the torque generated by collective pitch is considered to be a disturbance. It is also possible to identify the relation between yaw acceleration and collective pitch, in order to add compensation with the tail rotor as soon as collective pitch is applied. This compensation is not necessary since the INDI controller is able to quickly react to disturbances, as is shown in Section 6.2.

Since the INDI loop tracks a rotational acceleration in yaw, a PD-controller can be used to control the heading. The output of the PD-controller is the rotational acceleration reference for the INDI loop, as indicated in Fig. 4.

3.3. Effectiveness Matrix

The three control inputs for attitude control are cyclic roll θ_{1c}, cyclic pitch θ_{1s} and tail rotor command u_t. The controlled outputs are roll rate p, pitch rate q and yaw acceleration $\dot{r}$.

$$\boldsymbol{\nu} = \begin{bmatrix} \nu_p \\ \nu_q \\ \nu_{\dot{r}} \end{bmatrix}, \qquad \mathbf{y} = \begin{bmatrix} p \\ q \\ \dot{r} \end{bmatrix}$$

The assumption is made that the derivative of pitch and roll angles are equal to the pitch and roll rates in the body frame. This assumption is only valid for small angles, which are typical for normal helicopter flight.

The actuator effectiveness matrix $\mathbf{\Gamma}$ is constructed as follows:

$$\begin{bmatrix} p \\ q \\ \dot{r} \end{bmatrix} = \begin{bmatrix} G_{\theta_{1c}} & 0 & 0 \\ 0 & G_{\theta_{1s}} & 0 \\ 0 & 0 & G_{u_t} \end{bmatrix} \begin{bmatrix} \theta_{1c} \\ \theta_{1s} \\ u_t \end{bmatrix} \tag{31}$$

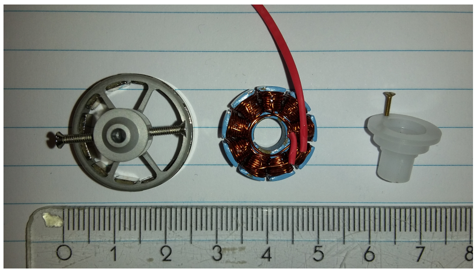

Figure 5: Glavak brushless direct drive motor and adapter piece.

For the INDI controller, the inverse of the effectiveness matrix is required, which is given by:

$$\mathbf{G}^{-1} = \begin{bmatrix} 1/G_{\theta_{1c}} & 0 & 0 \\ 0 & 1/G_{\theta_{1s}} & 0 \\ 0 & 0 & 1/G_{u_t} \end{bmatrix} \tag{32}$$

4. Helicopter Description

4.1. Base Helicopter

The helicopter used for this research project is the Walkera Genius CP V2 and is shown in Fig. 1. Without modifications and without battery, it weighs only 35 grams. Unlike most other toy helicopters in this class, the Walkera Genius CP V2 does not have a flybar for stabilization. It has built-in gyroscopes to stabilize attitude.

Specifications of the Walkera Genius CP V2:.

- Main rotor diameter: 240 mm
- Tail rotor diameter: 45 mm
- Nose-to-tail length: 220 mm
- Weight: 35 g
- Battery: 3.7V 200 mAh Li-Po

4.1.1. Brushless upgrade

By default, the helicopter is equipped with a brushed motor which drives the main shaft through gearing. Brushless motors have several advantages over brushed motors, including higher efficiency, less maintenance and better heat dissipation. Walkera offers a brushless upgrade kit to replace the brushed motor. With this upgrade kit, the gearing still remains. The plastic gears wear out quickly and are an extra source of vibrations.

Therefore, the helicopter is upgraded with a direct-drive brushless motor from Glavak. An adapter piece is made from nylon to attach the motor to the helicopter frame. A longer drive shaft is required to extend into the new motor. Figure 5 shows a picture of the stator and rotor of the Glavak motor and the nylon adapter piece.

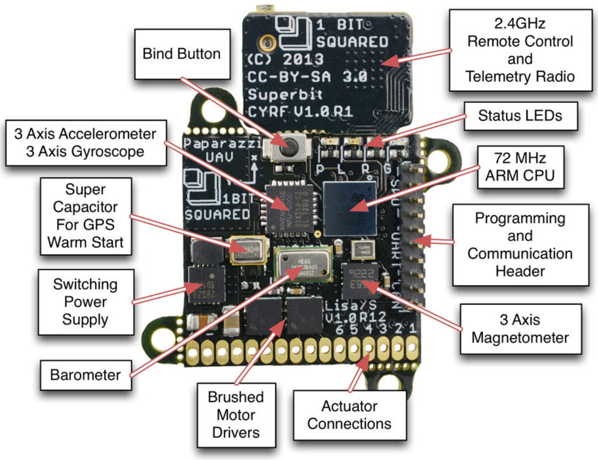

Figure 6: Lisa/S autopilot.

4.2. Autopilot

The standard electronics board cannot easily be reprogrammed and does not have the required sensors for attitude estimation. Therefore, the electronics board is replaced by a Lisa/S autopilot [15]. This autopilot was developed by the research group at the MAVLab and is shown in Fig. 6. By default it has a radio link which can also handle small telemetry messages. This radio link is removed to make room for a 4GB micro-SD card, which is soldered directly to the Lisa/S autopilot. The SD card can store measurement data at high speed and the data can be retrieved later. The new radio link uses a DSMX Deltang receiver, which requires only a single pin. Telemetry is done through an ESP-8266 WiFi chip, which requires only two free pins. The autopilot runs the attitude stabilization loop at 512 Hz.

Specifications of the Lisa/S autopilot:.

- Size: 2.0 x 2.0 x 0.5 cm
- Weight: 2.8 g
- Processor: 72MHz 32bit ARM Cortex M3 MCU with 16KB RAM and 512KB Flash
- IMU: InvenSense MPU-6050 3-axis gyroscope and 3-axis accelerometer
- Magnetometer: HMC5883L
- Barometer: MS5611
- GPS: ublox MAX-6 series

4.3. Actuators

The helicopter has three servo-actuators linked to the swashplate, visible in Fig. 7. The swashplate controls roll, pitch and thrust. A small DC motor on the tail provides control in yaw. This section describes the actuators and their characteristics.

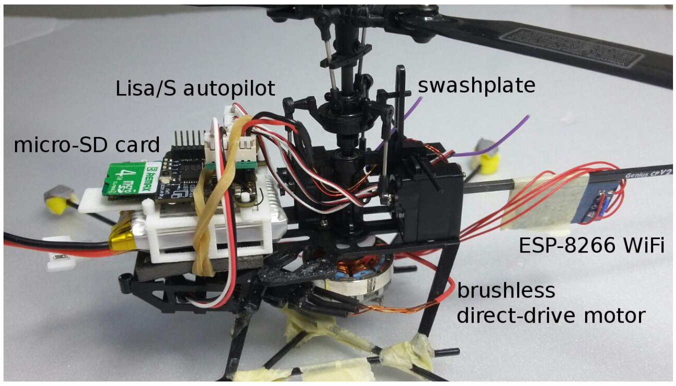

Figure 7: Close-up of the modified helicopter.

4.3.1. Measurement versus Model

In the inner feedback loop of INDI, the output of the actuator is required. The incremental command is added to the actuator output to obtain the new actuator command. The output can be either measured or estimated using a model. The steady-state output of the actuator needs to be equal to the actuator command, so the measurement needs to be mapped to the same unit as the command. If the mapping has an error, the steady-state output is not equal to the input command. The controller cannot correct for this error. As a result the output of the INDI control loop will have a steady-state error.

The problem with steady-state errors does not occur when using an actuator model. The model is guaranteed to have a steady-state gain of 1. Inaccuracies may exist in the model, but as shown in Section. 2.7, the output of the INDI controller still converges to the input.

4.3.2. Servo Actuator Model

The three servos are linked to the swashplate at 120° separation. The output of each servo is obtained by soldering a wire directly to the potentiometers inside the servo. Using the kinematics of the swashplate, the servo deflections are converted to pitch, roll and collective 'actuators'. The actuator model for pitch and roll is a combination of:

- A first order model with bandwidth 70 [rad/s].
- A fixed time-delay of 18 [ms].
- A rate saturation of 48 [-/s] (normalized)

This model accurately represents the measured deflection, as is shown in Fig. 8 for the pitch 'actuator'. To prevent steady-state errors, this model is preferred over direct measurements for actuator feedback in the INDI controller.

4.3.3. Tail Rotor Model

The tail rotor is driven by a brushed DC motor. It is assumed that thrust is linear with RPM and RPM is linear with applied voltage. These assumptions correspond to an error in the control effectiveness matrix. It is shown in Section. 2.6 that INDI can handle this type of error up to a certain level.

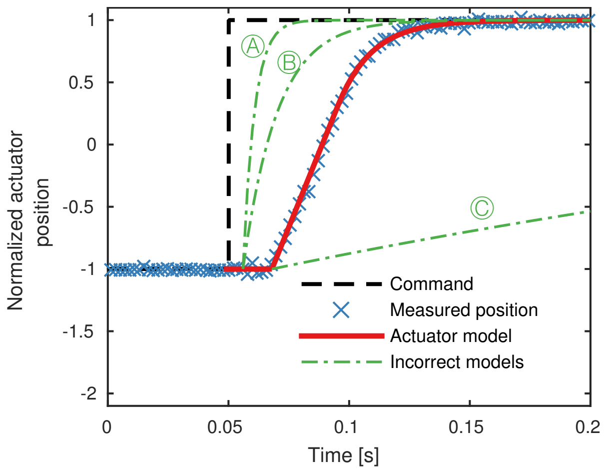

Figure 8: Model of the servo actuators.

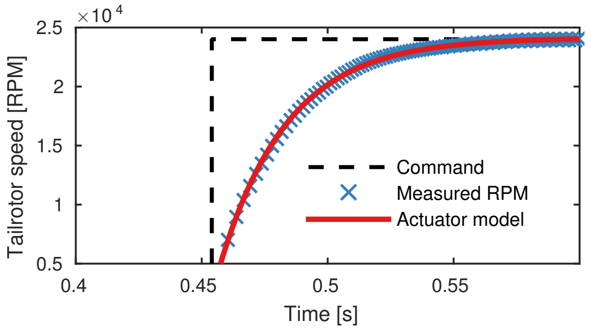

Figure 9: Model of the tail rotor spinning up. $\omega_c = 37$ rad/s.

Since it is not possible to measure the RPM during flight, a model has to be used. The RPM was measured with an infrared tachometer in a static setup. It was found that there is a significant difference between the motor spinning up and down. Both directions are modeled as a first order system, but with different bandwidths. The bandwidth is 37 rad/s while spinning up and 13 rad/s when spinning down. Figure. 9 and Fig. 10 show the response to step inputs in both directions.

The model diverges at low RPM when the motor is spinning down. However in normal flight conditions, the RPM is not expected to reach such low values. It is more

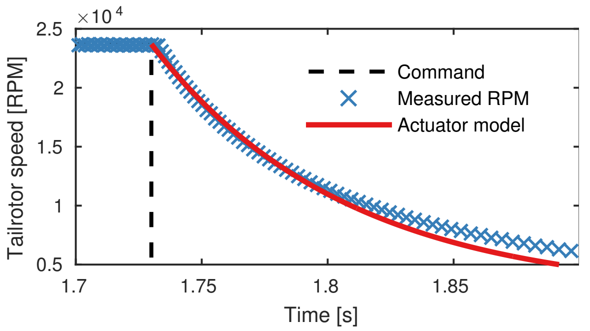

Figure 10: Model of the tail rotor spinning down. $\omega_c = 13$ rad/s.

important that the model is accurate around the trim condition, which is at approximately 80% of the maximum RPM.

5. Control Effectiveness Identification

While the actuator models could be identified without flying, the control effectiveness can only be identified by performing in-flight experiments. That is not trivial however, since the result of the identification are necessary for stabilization. One way to overcome this dependency loop is to use adaptive INDI, as proposed by Smeur et al. [12]. The control effectiveness needs to be initialized with some values of which the signs must be correct. For a large range of initial values, the adaptive algorithm lets the control effectiveness converge to flyable values before the UAV crashes.

For the control effectiveness identification this section, the helicopter is initially stabilized with PID controllers. The PID controllers do not need to be tuned for best performance, because they will be replaced by INDI. Small disturbance signals are injected during flight and the relations between actuator commands and output measurements can be identified. This method is preferred over the adaptive approach for better repeatability.

The Linear Least Squares (LLS) algorithm is applied to derivatives of both inputs and outputs to find the effectiveness. The use of derivatives eliminates the offset. This reduces the number of parameters to fit when applying LLS.

5.1. Pitch and Roll

The relations between cyclic inputs with pitch and roll rate are modeled as:

$$\Delta p = \Gamma_{\theta_c} A_p(z) \Delta\theta_c \tag{33}$$

$$\Delta q = \Gamma_{\theta_s} A_q(z) \Delta\theta_s \tag{34}$$

where $A_p(z)$ and $A_q(z)$ represent the output of a nonlinear model of the combined actuator dynamics from Section 4.3.2 and first-order damping as explained in Section 3.1.1. The actuator model is known, but the bandwidth of the first-order damping is still unknown.

A disturbance signal is constructed as a sum of four sine-waves, at frequencies of 2, 4, 6 and 8 Hz. A phase-shift is applied at each frequency to limit the maximum amplitude of the combined signal. The disturbance is added to the stabilization command. An ideal low-pass filter of 10 Hz is applied to the output of the combined actuator dynamics and first-order damping model. The same filter is applied to the roll and pitch rate measurements.

To find the bandwidth of the first-order damping dynamics, the linear least squares method is applied for all bandwidths in the range from 1 to 200 rad/s. The bandwidth is found where the remaining squared error is the smallest. In roll, the damping bandwidth is 68 rad/s. The

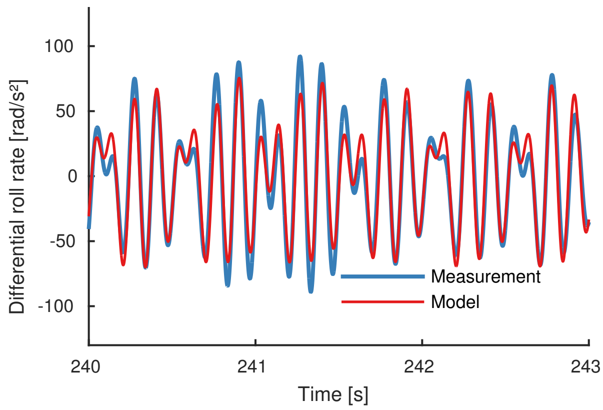

Figure 11: Roll identification

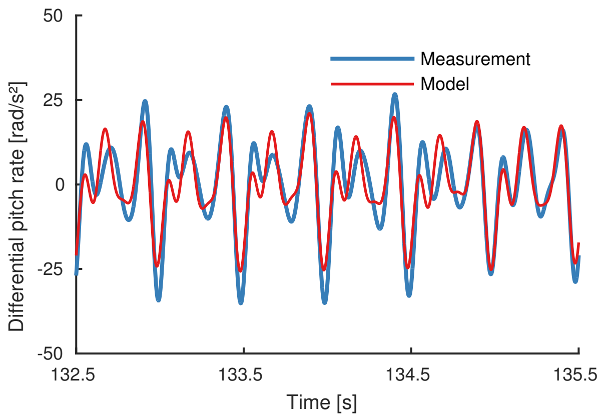

Figure 12: Pitch identification

damping in pitch is slower with a bandwidth of 17 rad/s. The difference can be explained by the difference in inertia in pitch and roll. Due to higher inertia in pitch, it takes longer to reach a steady-state pitch rate.

The correction factors as described in Section. 3.1.2 are found imperically as $F_{\theta_{1s}} = 0.19$ and $F_{\theta_{1c}} = -0.58$. Each pitch command is accompanied by a roll command which is 19% the magnitude of the pitch command. Every roll command is accompanied by a negative pitch command of 58% the magnitude in roll. Without these compensations, the helicopter is also able to stabilize but with slow oscillations. A better identification method for the compensation parameters is left for future work.

5.2. Yaw

A direct relation is assumed between change in tail-rotor speed u_t and change in yaw acceleration $\dot{r}$, such that:

$$\Delta u_t \cdot \Gamma_{u_t} = \Delta \dot{r} \tag{35}$$

where Γ_{u_t} is the control effectiveness. The true RPM of the tail rotor is not required. For convenience, it is normalized such that $u_t \in [0, 1]$. The normalization only results in a scaling of the control effectiveness.

Similar to the identification procedure in pitch and roll, a disturbance signal is added to the stabilization command. This signal also consists of four sine-waves at 2, 4, 6 and 8 Hz. A change in collective pitch also causes acceleration in yaw and is therefore carefully trimmed. The trimming of collective allows the helicopter to hover steadily for a period of several seconds, while the disturbance signal is injected.

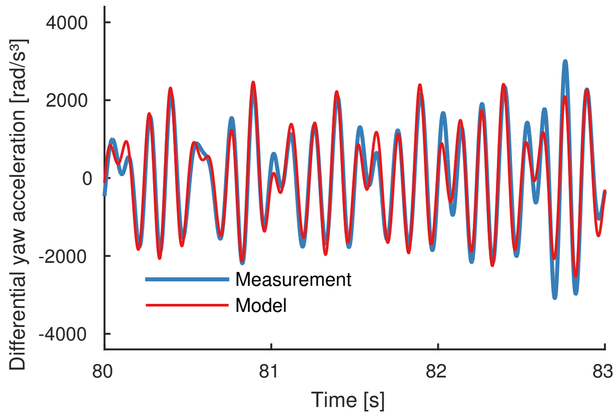

Figure 13: Tail rotor to yaw acceleration effectiveness model.

The tail-rotor speed cannot be measured directly, but is calculated by applying the model from Section 4.3.3 to the tail-rotor input signal c_t. A non-causual low-pass filter is applied to the reconstructed tail-rotor speed with a cutoff frequency of 10 Hz. The same filter is applied to the differentiated yaw rate measurements. The cutoff frequency at 10 Hz allows the results of the disturbance to appear in the measurement, while high frequency noise is excluded.

The effectiveness is obtained by applying LLS. Figure 13 shows that the model is an accurate estimate of the real helicopter in hovering conditions. The model is also used in other flight conditions, assuming that INDI is able to resolve the model mismatch.

6. Results and Discussion

This section shows the performance of the INDI attitude controller on the small helicopter UAV. Only the roll and yaw directions are explored here, since the properties of the controller in pitch are very similar to roll.

6.1. Roll Performance

To evaluate the control performance in roll, the helicopter is commanded to follow a doublet reference signal.

A simple PD-controller is used as a reference for a qualitative performance analysis. The goal here is not to determine which controller is 'better' or 'faster', but to show that INDI has some properties which are not present in a simple PD-controller.

Figure 14a shows the response of the PD-controlled helicopter to a doublet roll reference. The PD-controller shows a steady-state offset which is not present with INDI in Fig. 14c. The offset is caused by a slight misalignment of the servo's. When a roll command of zero is given,

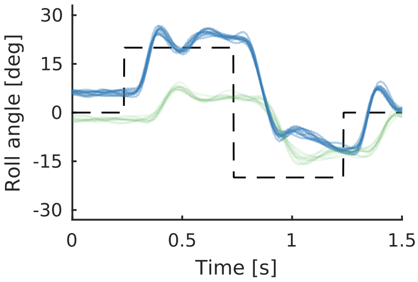

(a) Doublet response with PD-controller.

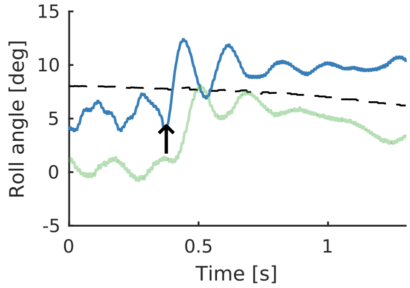

(b) Disturbance rejection with PD-controller.

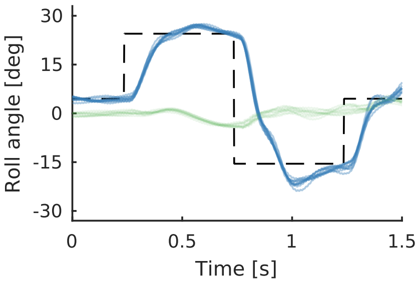

(c) Doublet response with INDI controller.

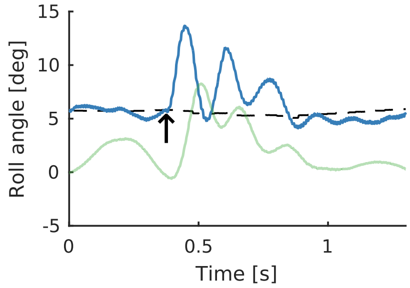

(d) Disturbance rejection with INDI controller.

Figure 14: Roll angle response to a doublet input and a disturbance with a PD- and an INDI controller. The reference is marked by the dashed line. The blue lines represent the roll angle. The light-green lines represent the pitch angle.

the swashplate is slightly tilted causing the helicopter to roll. Adding an integral to the PD-controller could also eliminate this error, but this would also affect the input tracking dynamics. INDI does not have steady-state errors as shown in Section. 2.

The reference signal for the doublet with INDI has an offset of 4.5°, while this is not present in the PD-controller. A roll angle of approximately 4.5° is required to compensate sideways drift caused by the tail rotor force. Since the PD-controller has a steady-state error, the reference signal is lowered. Otherwise, the helicopter would rapidly drift to the right during the experiment.

During the doublet, the pitch angle is commanded to stay zero. With both controllers, the simple decoupling compensations as described in Section. 3.1.2 are applied. The PD-controller shows a steady-state error in pitch which appears to be proportional to the roll angle. The incremental loop inside INDI already compensates quickly for errors in pitch rate. Also, the INDI controller does not give a steady-state error in the pitch angle.

Figures 14b and 14d show the roll angle response after a step disturbance. Before the disturbance, the helicopter carries a weight of 4.5 grams with a string at an offset of 4.5 cm from the center of gravity. By cutting the string, the weight is removed instantaneously.

For the disturbance experiments, the helicopter is commanded to hover in the OptiTrack arena using a PD-controller for horizontal guidance. The guidance controller generates the pitch and roll reference angles. Because the weight is on the left, the steady-state error with the PD-controller is to the left. The guidance controller commands a higher roll angle to make the helicopter hover. Before the weight is cut, there are oscillations in roll. The PD-controller has difficulties stabilizing with the weight attached. After the weight is cut, the roll rate is damped and the roll angle stabilizes with a different steady-state error.

The INDI controller has no steady-state error while tracking the roll angle reference in Fig. 14d. According to the theory in Section 2.5, a disturbance in roll rate is damped out with the dynamics of the actuator and the measurement filter. In this case, the measurement filter is a second order Butterworth filter with a cut-off frequency of 40 Hz combined with a second order notch filter at the frequency of the main rotor.

When the disturbance is applied by cutting the string, the response does not show nice damping with INDI. Instead, the roll angle is strongly oscillating. It appears to be coupled with the pitch motions. The simple decoupling strategy as explained in Section 3.1.2 helps to some extent in reference tracking as is visible in Fig. 14c. However in disturbance rejection, it is counterproductive. The disturbance causes the roll rate to increase, which is counteracted by INDI by giving a negative command in roll. The simple decoupling mechanism then also sends a positive command to pitch, which makes the pitch angle increase. The positive pitch rate is compensated with negative pitch command, but also a negative roll command. This results in a roll rate which is more negative than the reference from the P-controller. The roll rate is continuously overshooting the roll rate reference due to the coupling with pitch. This is believed to be the main cause of the oscillations.

6.2. Yaw Performance

For heading control, the difference is shown between a simple PD-controller and INDI. The PD-controller also has a feed-forward component related to the thrust command. The PD-controller shows a large steady-state error in Figures 15a and 15b. This can be attributed to bad tuning of the feed-forward component and lack of an integral in the controller. Ten doublets were performed on the same battery with several seconds in between. It was found that the steady-state error increases when the battery voltage gets lower.

The PD-gains used in the INDI controller are set such that the dynamic response is relatively close to that of the PD-controller. By doing so, it is more clearly visible how the controllers differ in disturbance rejection. The disturbances in yaw are applied by adding a significant amount of collective for half a second. This also generates additional torque which needs to be compensated by the tail rotor. The INDI controller performs much better here since it feeds back rotational acceleration internally, while the PD-controller feeds back the rotational rate.

The INDI controller is able to recover from the first disturbance before the second disturbance occurs. During this maneauvre, the tail rotor has to spin up quickly. After the second disturbance it takes more time to recover. This time, the tail rotor needs to slow down and it was shown in Section 4.3.3 that the dynamics of the tail rotor spinning down are slower. Therefore the disturbance rejection is also slower, according to Eq. 20.

Also in the doublet on the heading reference in Fig. 15c, a clear difference can be seen between the directions of yaw. For a heading increase, the tail rotor has to spin up and it has to slow down for a decrease in heading. This results in faster or slower dynamics in the heading control loop.

Another interesting observation is the steady-state error with the INDI controller in Figs. 15c and 15d. According to Eq. 29, there should be no steady-state error as long as the actuator model has no steady-state error. In this case, two different models are used to represent the tail rotor for spinning up and down. When the acceleration error is close to zero, the INDI controller is rapidly switching between these two models. It was found that when only a single model is used, either the faster or the slower one, the steady-state error is actually zero.

6.3. Actuator Model Mismatch

It is not always possible to find an accurate model of the actuators. In case of this helicopter, the roll damping dynamics are also included in the actuator model. These damping dynamics are difficult to estimate. The following experiment is designed to evaluate the effects of an incorrect actuator model.

The response to a doublet input on the roll angle is measured for different incorrect actuator models. In all cases, the P-gain is 12. The control effectiveness as identified in Section 5.1 is used. The fast damping dynamics are not included in the actuator models in these experiments.

The step responses of the incorrect actuator models are included in Fig. 8. The faster model (B) is a first order system with a bandwidth of 70 rad/s and a fixed delay of 6 ms. The slower actuator model (C) has a bandwidth of 2 rad/s and a fixed delay of 18 ms. The experiment is repeated 10 times for both configurations.

In Fig. 16c, the helicopter slowly follows the reference angle in roll. This behavior corresponds to the theory in Section 2.7. Because the model is slower, the new control input to the system is lower. The steady-state error should still be zero according to theory. This is also observed in the experiment.

Figure 16b shows the helicopter tracking the roll reference with a faster actuator model in the loop. The output of the model is faster, resulting in a higher control input to the system. According to theory, this results in a second order under-damped system for the roll rate. These oscillations also show up in the roll angle. Despite the oscillations, the roll angle still follows the reference with zero steady-state error.

The final experiment in this category is designed to show stability with an even faster actuator model (A), which has a bandwidth of 210 rad/s and a fixed delay of 6 ms. In this experiment, only a slowly varying roll angle reference is tracked. The result is shown in Fig. 16a. Theoretically, the roll rate still has zero steady-state error. However in this case, the P-controller is continuously changing the roll rate reference ν_p according to the error in roll angle. The combination results in a continuously oscillating system response.

6.4. Control Effectiveness Mismatch

The estimated control effectiveness may not be accurate or not applicable to a large part of the flight envelope. The following experiment explores the effect of model mismatch in the control effectiveness matrix on the roll axis. The input signal is a doublet on the roll angle reference. In the nominal case, the control effectiveness found in Section 5.1 is used. In the underestimated case, the control effectiveness is half of the nominal value. In the overestimated case, the control effectiveness is selected twice the value of the nominal case. These values represent large errors in the estimated effectiveness.

Also the P-gain of the attitude command loop is varied between three different values. The gains are selected to be in the flyable range for all three control effectiveness values. With the lowest P-gain, the helicopter responds slowly to attitude commands, which makes it difficult to

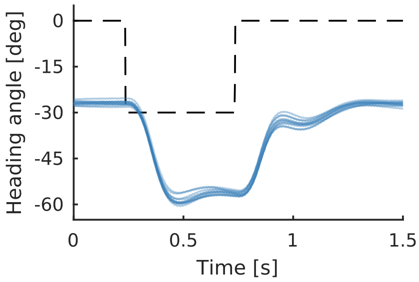

(a) Doublet response with PD-controller.

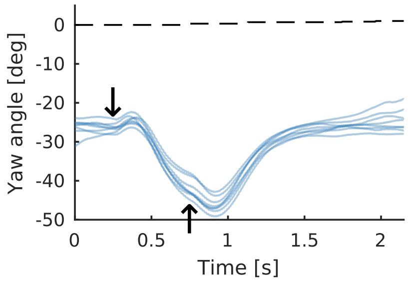

(b) Disturbance rejection with PD-controller.

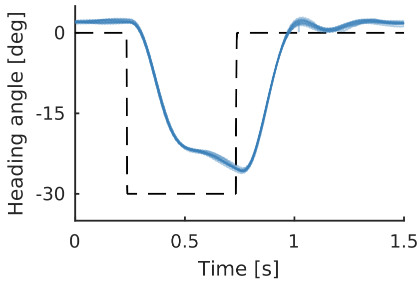

(c) Doublet response with INDI controller.

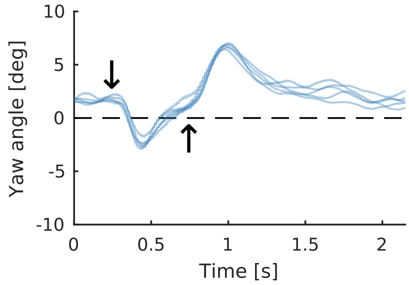

(d) Disturbance rejection with INDI controller.

Figure 15: Heading response to a doublet input and a disturbance with a PD- and an INDI controller. The reference is marked by the dashed line. The blue lines represent the heading.

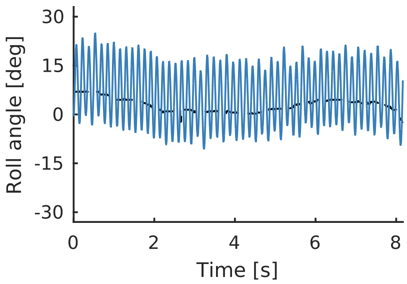

(a) Faster actuator model: $\omega_c = 210$ rad/s and fixed time delay of 6 ms.

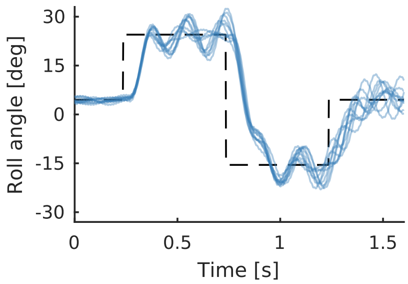

(b) Faster actuator model: $\omega_c = 70$ rad/s and fixed time delay of 6 ms.

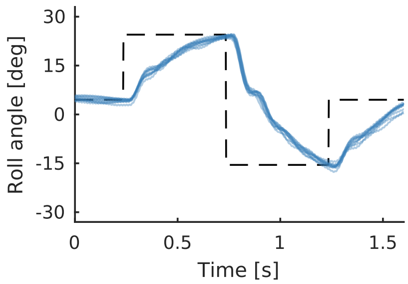

(c) Slower actuator model: $\omega_c = 2$ rad/s and fixed time delay of 18 ms.

Figure 16: Tracking a reference signal with different incorrect actuator models within the feedback loop in INDI. The dashed line shows the reference. The blue lines represent the roll angle.

control. The highest P-gain is selected at a value where the helicopter begins to show some oscillations.

The experiment is repeated 10 times for each set of parameters, which provides insight in the repeatability. With the OptiTrack system, the experiment is performed completely autonomous. The altitude is controlled with a PID-controller on collective and a feed-forward term depending on the roll angle. During every experiment, the pitch angle is controlled by INDI with the nominal effectiveness as identified in Section 5.1 and a P-gain of 8.

The response of the helicopter is first estimated in a simulation, by simply replacing the INDI loop with Eq. 21 for a single degree of freedom. The under- and over-estimated effectivenesses are modeled with K_c. The simulated response is shown by the red lines in Fig. 17.

Figures 17a-17c show the responses for the overestimated actuator effectiveness. As a result of this, the INDI loop follows the reference roll rate with a delay larger than the actuator dynamics. Increased delay results in an increased overshoot. The overshoot also increases with a larger P-gain, which also happens in the simulations.

There is also a notable difference between the measured and simulated responses. Also within the 10 experiments per parameter set, there is some variation. The simulation response should not be misinterpreted for a reference signal. Small differences in the beginning will result in larger differences later on. Because the effectiveness is overestimated, only small control inputs are given to track the

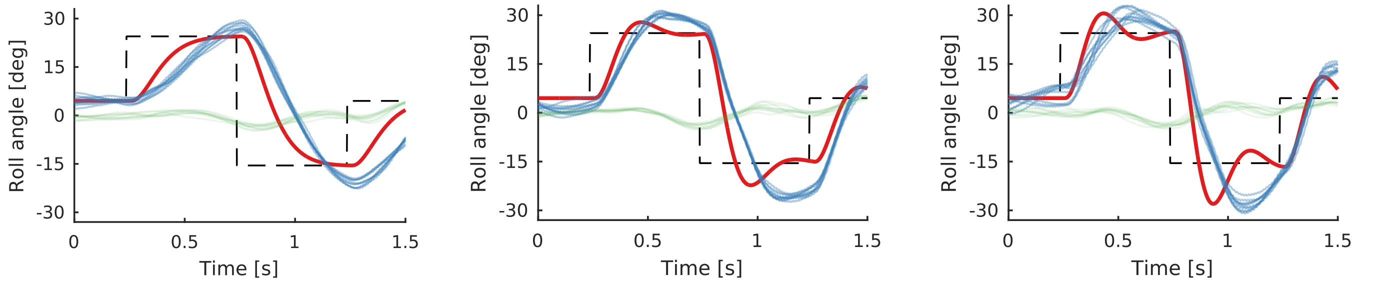

(a) Control effectiveness = 200%, P = 6 (b) Control effectiveness = 200%, P = 12 (c) Control effectiveness = 200%, P = 16

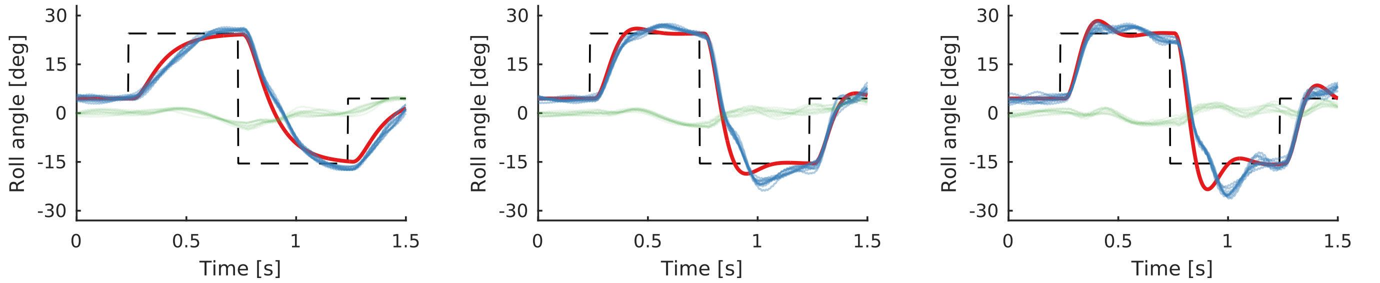

(d) Control effectiveness = 100%, P = 6 (e) Control effectiveness = 100%, P = 12 (f) Control effectiveness = 100%, P = 16

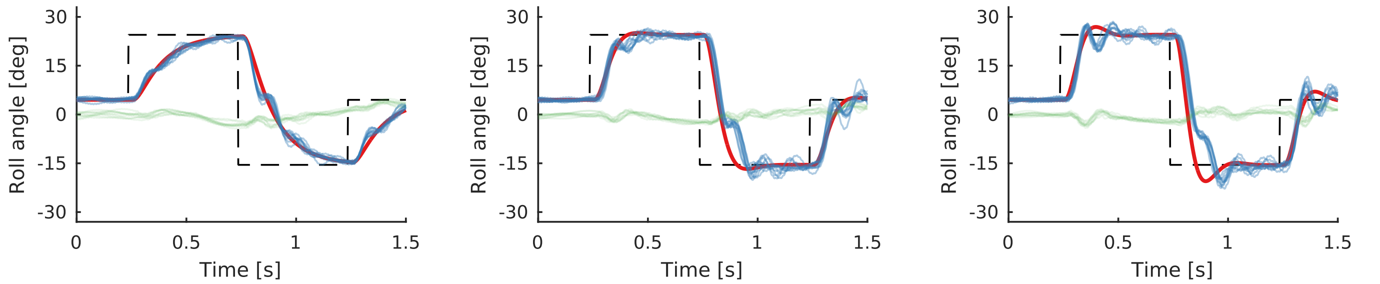

(g) Control effectiveness = 50%, P = 6 (h) Control effectiveness = 50%, P = 12 (i) Control effectiveness = 50%, P = 16

Figure 17: Response to a doublet input reference on the roll angle for various values of control effectiveness and different P-gains for the attitude control loop. The reference is marked by the dashed line. The blue lines represent the roll angle. The light-green lines represent the pitch angle. The red lines show the simulated system in response to the reference.

reference and reject disturbances. The ratio of control input to disturbances is smaller compared to the nominal case. Each test run has slightly different disturbances, resulting in an observable difference in the response.

The measured response in the nominal case is in line with the expectations, with only one exception. Especially with the higher P-gains in Figs. 17e and 17f, a dip is observed in the roll rate during the step from 24.5° to -15.5°. It can also be observed in Figs. 17h and 17i. This is most likely related to the high magnitude of the roll rate, since it is not observed during the initial smaller step. This behavior is not studied further, since it only occurs when the step is large and it only results in a slightly slower response.

With the underestimated effectiveness in Figs. 17g-17i, the INDI controller responds about twice as fast to errors in the roll rate. In Fig. 17g, the low P-gain provides a relatively slow roll rate reference, which is quickly followed by the INDI loop. Instead of just following the reference twice as fast, the INDI loop also introduces oscillations. The frequency of these oscillations is independent of the P-gain, although the amplitude increases with higher P-gains.

A possible explanation for these oscillations is a slightly incorrect actuator model. Although it is not proven in this paper, it is expected that errors in the actuator model introduce larger errors in tracking if the effectiveness is underestimated. Even though the actuator model matches well with measurements, it must be considered that the measurement was performed on the ground with no loads applied. It is very well possible that the actuators behave (slightly) different during flight. Section 2.7 shows that a faster actuator model results in oscillations. Taken into consideration that the oscillations due to the faster actuator model are amplified by the underestimated actuator effectiveness, this might explain the oscillations observed in Figs. 17g-17i.

7. Conclusions and Recommendations

An INDI attitude controller was proposed which controls pitch- and roll rates directly, instead of accelerations. The fast transient dynamics were accounted for in the same way as actuator dynamics. The new controller was implemented on a small modified Walkera Genius CP V2 helicopter. It was shown that with this method, it is possible to find a control effectiveness matrix with just three constants. This is much simpler than previously proposed implementations of INDI on helicopters. Despite the simplicity, the controller was able to track a reference signal similarly to the simulated response. The disturbance rejection capabilities of the controller were also demonstrated. The robustness of the controller was tested by experimenting with deliberately incorrect values for the control effectiveness matrix and actuator model. The helicopter could successfully be controlled over a wide range of incorrect parameters. It can be concluded that the attitude controller presented in this paper is a suitable choice for small autonomous helicopters.

The main difficulty in configuring the controller now is to find the control effectiveness values, which has to be done in flight. As a recommendation for future work, an adaptive algorithm can be implemented as was already demonstrated by Smeur et al. [12] on a quadcopter. The actuator model can already be determined on the ground and the calculation of the PD gains can also be done without flying. The adaptive algorithm would make the controller work from the first flight.

It is also suggested that the couplings in pitch and roll are examined in more detail, so that the decoupling strategy can be improved and parameters can be identified online. Also, the controller now only controls the attitude. This can be extended to vertical acceleration which would also allow to decouple yaw from thrust more effectively.

Acknowledgements

The authors would like to thank the people in the MAVLab for their enthusiasm and support and T. Cunis for helping out with linear algebra.

References

[1] S. Driessens and P. E. I. Pounds. Towards a more efficient quadrotor configuration. In *Intelligent Robots and Systems (IROS), 2013 IEEE/RSJ International Conference on*, pages 1386–1392, Nov 2013. doi: 10.1109/IROS.2013.6696530.

[2] Luis Mejías, Srikanth Saripalli, Pascual Campoy, and Gaurav S. Sukhatme. Visual servoing of an autonomous helicopter in urban areas using feature tracking. *Journal of Field Robotics*, 23, 2006.

[3] S. Saripalli, J.M. Roberts, P.I. Corke, G. Buskey, and G. Sukhatme. A tale of two helicopters. In *Intelligent Robots and Systems, 2003. (IROS 2003). Proceedings. 2003 IEEE/RSJ International Conference on*, volume 1, pages 805–810 vol.1, Oct 2003. doi: 10.1109/IROS.2003.1250728.

[4] T.J. Koo and S. Sastry. Output tracking control design of a helicopter model based on approximate linearization. In *Decision and Control, 1998. Proceedings of the 37th IEEE Conference on*, volume 4, pages 3635–3640 vol.4, Dec 1998. doi: 10.1109/CDC.1998.761745.

[5] K. Sprague, V. Gavrilets, D. Dugail, B. Mettler, E. Feron, and I. Martinos. Design and applications of an avionics system for a miniature acrobatic helicopter. In *Digital Avionics Systems, 2001. DASC. 20th Conference*, volume 1, pages 3C5/1–3C5/10 vol.1, Oct 2001. doi: 10.1109/DASC.2001.963353.

[6] V. Gavrilets, A. Shterenberg, I. Martinos, K. Sprague, M.A. Dahleh, and E. Feron. Avionics system for aggressive maneuvers. *Aerospace and Electronic Systems Magazine, IEEE*, 16 (9):38–43, Sep 2001. ISSN 0885-8985. doi: 10.1109/62.949536.

[7] Zhe Jiang, Jianda Han, Yuechao Wang, and Qi Song. Enhanced lqr control for unmanned helicopter in hover. In *Systems and Control in Aerospace and Astronautics, 2006. ISSCAA 2006. 1st International Symposium on*, pages 6 pp.–1443, Jan 2006. doi: 10.1109/ISSCAA.2006.1627508.

[8] Eric Johnson, , Eric N. Johnson, and Daniel P. Schrage. The georgia tech unmanned aerial research vehicle: Gtmax. In *in Proceedings of the AIAA Guidance, Navigation, and Control Conference*, pages 2003–5741, 2003.

[9] Jesse Leitner, Anthony Calise, and J.V.R. Prasad. Analysis of adaptive neural networks for helicopter flight controls, 1995.

[10] B. Schölkopf, J. Platt, and T. Hofmann. *An Application of Reinforcement Learning to Aerobatic Helicopter Flight*, pages 1–8. MIT Press, 2007. ISBN 9780262256919.

[11] S. Sieberling, Q. P. Chu, and J. A. Mulder. Robust flight control using incremental nonlinear dynamic inversion and angular acceleration prediction. *Journal of Guidance, Control, and Dynamics*, 33(6):1732–1742, Nov 2010. ISSN 0731-5090. doi: 10.2514/1.49978.

[12] E.J.J. Smeur, Q.P. Chu, and G.C.H.E de Croon. Adaptive nonlinear dynamic inversion for attitude control of micro aerial vehicles. *Journal of Guidance, Control and Dynamics*, 2015.

[13] P. Simplicio, M. D. Pavel, E. van Kampen, and Q. P. Chu. An acceleration measurements-based approach for helicopter nonlinear flight control using incremental nonlinear dynamic inversion. *Control Engineering Practice*, 21(8):1065–1077, 2013. doi: 10.1016/j.conengprac.2013.03.009.

[14] B. J. Bacon, A. J. Ostroff, and S. M. Joshi. Reconfigurable ndi controller using inertial sensor failure detection amp; isolation. *IEEE Transactions on Aerospace and Electronic Systems*, 37(4):1373–1383, Oct 2001. ISSN 0018-9251. doi: 10.1109/7.976972.

[15] B. D. W. Remes, P. Esden-Tempski, F. Van Tienen, E. Smeur, C De Wagter, and G. C. H. E. De Croon. Lisa-s 2.8g autopilot for gps-based flight of mavs. *Proceedings 2014 IMAV*, pages 280–285, Aug 2014.

Part II

Additional Work

Chapter 1

Attitude Estimation

The most commonly used methods for attitude estimation on UAVs rely on combined gyroscope and accelerometer measurements. Gyroscopes measure the angular velocities and an attitude estimate is obtained from integration. However, small errors in angular velocity measurement will integrate towards large errors in the attitude estimate. The drift is compensated with accelerometer measurements. Among other accelerations and noise, accelerometers measure the direction of the gravity vector. The pitch and roll angle can be obtained from the direction of the gravity vector in the body frame. It is impossible to distinguish gravity from other accelerations. However in most flight conditions, the average of acceleration measurements represents gravity. In these conditions it is possible to obtain an attitude estimate by applying a fusion algorithm.

1-1 Fusion algorithms

The basic concept of an attitude state estimation algorithm is to combine measurements of two or more sensors, using only the reliable frequencies of each sensor, to provide a reliable signal over the entire bandwidth. To achieve a reliable attitude estimate, the low-frequency data of the accelerometers can be combined with high-frequency data from gyroscopes.

Two types of filters are found in literature: Kalman filters **?** and a complementary filters **?**. A Kalman filter can be either direct or indirect. The state vector of a direct Kalman filter contains all the variables of interest, while an indirect Kalman filter holds only an error-state.

The three variations of complementary filters are direct, passive and explicit Mahony et al. (2008). The difference between the direct and passive complementary is the reference frame in which the gyroscope measurements are integrated. The direct filter uses the reference frame which is constructed directly from the accelerometer measurements. The passive filter uses the estimated reference frame itself in a feedback structure. The direct variation is more sensitive to accelerometer noise, since gyroscope measurements are integrated in a reference frame that is constructed from noisy accelerometer measurements.

The explicit complementary filter does not construct a frame of reference to propagate the gyroscopes. Thereby it saves some computations. It is a reformulation of the passive complementary filter in terms of direct measurements from the inertial sensors Mahony et al. (2008).

In general, the performance of a Kalman filter is better, but so is the computational burden Carminati et al. (2012). Considering the limited computational power on the Lisa/S autopilot and 'good' performance of complementary filters in literature **????**, the explicit complementary filter is chosen as the attitude estimation algorithm.

1-2 Explicit Complementary Filter

An explicit complementary filter, as described by Mahony et al. (2008), is implemented using a quaternion state representation. This representation can be implemented more efficient than Euler angles or direction cosines. The processor on the Lisa/S has no Floating Point Unit (FPU) or Digital Signal Processor (DSP). Therefore an implementation using integers is used.

The explicit complementary filter consists of the following set of equations, which is cited directly from Mahony et al. (2008):

$$\omega_{\text{mes}} = -\text{vex}\left(\sum_{i=1}^{n} \frac{k_i}{2}\left(v_i \hat{v}_i^T - \hat{v}_i v_i^T\right)\right) \tag{1-1}$$

$$\dot{\hat{q}} = \frac{1}{2}\hat{q} \otimes \mathbf{p}\left(\Omega_y - \hat{b} + k_P \omega_{\text{mes}}\right) \tag{1-2}$$

$$\dot{\hat{b}} = -k_I \omega_{\text{mes}} \tag{1-3}$$

The correction term ω_{mes} is an approximation of the error as measured from the current estimate. The vector v_i represents a measurement of a known inertial direction, such as gravity and the local magnetic field. $\hat{v}_i$ is the estimated direction of the vector in the current estimate. Each of these vectors can have its own associated gain k_i according to the confidence in the sensor. For attitude estimation on the helicopter, only the gravity vector is used. In case of only one inertial vector, Eq. 1-1 is effectively a cross product of the measurement with its estimate:

$$\omega_{\text{mes}} = -\frac{1}{2} v_g \times \hat{v}_g \tag{1-4}$$

where v_g is the gravity vector and $\hat{v}_g$ is its current estimate.

The rotational rate of the estimate of the attitude quaternion $\dot{\hat{q}}$ consists of the gyroscope measurements Ω_y, the estimate of gyroscope bias $\hat{b}$ and a correction term multiplied by a proportional gain k_P. These rotational rates are considered to be in the current estimate. The estimate of the gyroscope bias $\hat{b}$ is not constant. Its rate of change is proportional to the correction term ω_{mes} and an integral gain k_I. For a more detailed explanation of the explicit complementary filter, the reader is referred to Mahony et al. (2008).

1-3 Vibrations

Vibrations are also measured as accelerations. While vibrations are often misinterpreted as noise, the accelerometer is actually accelerating due to vibrations. Since the average of vibrations is zero, the average of the accelerometer measurements should represent the average of the gravity vector.

Using the explicit complementary filter from Mahony et al. (2008), the part of the correction term ω_{mes} as a result of vibrations does not average to zero. This is caused by the normalization of the measured acceleration, by which only the information of the angles is retained.

The solution implemented here is to not normalize the acceleration measurements. In this case, the correction term from any pair of measurements separated by half the vibration period is equal in magnitude and opposite in direction. A correct average is thereby guaranteed. The downside of this method is that the the magnitude of the correction term increases when the magnitude of vibration increases.

The the correction term is also increased in situations where the helicopter is accelerating. Then, the accelerometers measure the sum of gravity and acceleration and the direction of the accelerometer measurement does not necessarily represent that of gravity. The higher correction term causes the filter to correct faster towards the wrong value, which is off course undesired.

1-4 Accelerations

The the correction term ω_{mes} is also increased in situations where the helicopter accelerates. Then, the accelerometers measure the sum of gravity and acceleration and the direction of the accelerometer measurement does not necessarily represent that of gravity. A higher correction causes the filter to correct faster towards the wrong value, which is off course undesired.

If the flight profile only contains short periods of accelerations, the explicit complementary filter is still able to present an accurate estimate of attitude. The adjectives short and accurate will be quantified in an experiment.

1-5 Performance Evaluation

The performance of the complementary filter is compared with the attitude measured by OptiTrack™, an optical motion tracking system using reflective markers. The flight area is limited to 10m x 10m x 10m. Within this area, it is only possible to accelerate for a short amount of time. This technique cannot be applied to verify the attitude estimation performance for a normal outdoors mission.

Experiment setup

In the first experiment, the helicopter is simply commanded to hover at a fixed position directly after takeoff. The position control loop is a PID-controller. The attitude controller

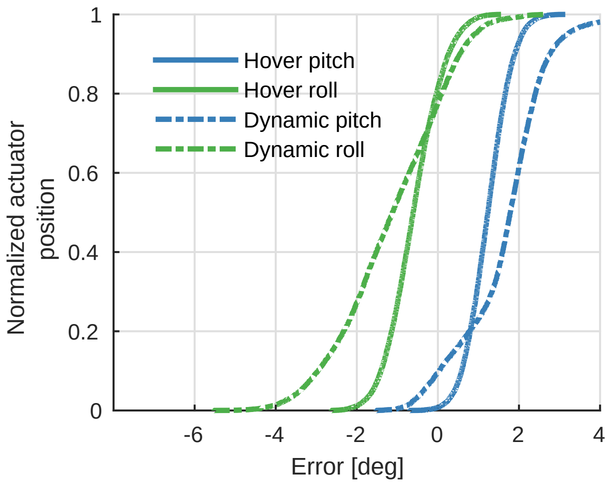

Figure 1-1: Cumulative distribution function of pitch and roll error. Hover data is collected for a period of 216 s. Dynamic data is collected during 192 s in which the trajectory was flown 12 times.

is an Incremental Nonlinear Dynamic Inversion (INDI)-controller with non-optimal gains. These non-optimal gains result in small oscillations, which are quite useful in evaluating the performance of the complementary filter.

The second experiment is designed to evaluate the influence of accelerations on the attitude estimate. Instead of hovering, the helicopter is commanded to fly back and forth between two points located 6.75 m apart. The helicopter hovers at each point for approximately 4 seconds while changing the heading to face towards the other point. Then it is commanded to fly to the other point with a velocity of 2.0 m/s. The same controllers are used for attitude and position.

The metrics used for attitude estimation performance are the error in pitch and roll angle. The difference between the two experiments can be attributed to the maneuvers performed by the helicopter.

Results and Discussion

Figure 1-1 shows the cumulative distribution functions of the two experiments in one graph. During the first experiment, when the helicopter hovers for 216 seconds, the pitch error is bounded between approximately zero and three degrees. The pitch angle shows an average offset of 1.5 degrees. The error in roll shows similar characteristics during hover, but with a different offset. Errors between ± 3 degrees in pitch and roll are considered to be sufficient for autonomous flight. Actually, during the hover experiment, the helicopter managed to stay within a radius of 6 cm from the waypoint using a simple PID position controller.

The attitude estimation performance is somewhat degraded during the second experiments, in which the helicopter continuously flies back and forth between two waypoints. The cycle is repeated 12 times in 192 s. Figure 1-2 shows the pitch and roll errors together with the position along the track. At points (1), (3) and (5), the helicopter hovers at one waypoint and quickly yaws 180° to make the nose point towards the other waypoint. During this turn,

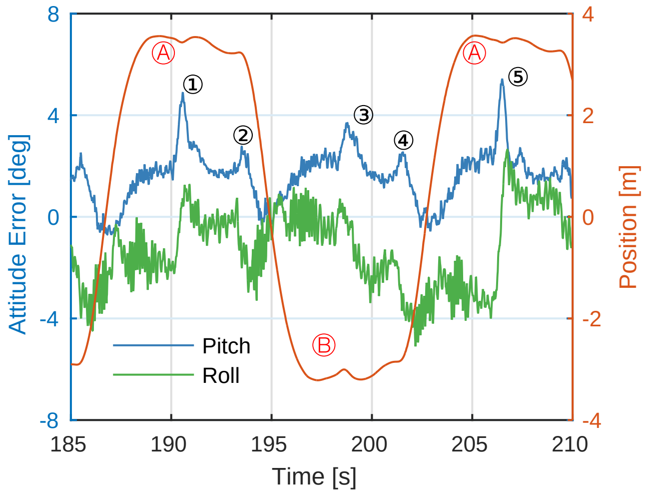

Figure 1-2: Attitude error in pitch and roll during the 6th cycle of a flight between two waypoints.

the tail rotor generates a sideways acceleration which is compensated by the position control loop by rolling and pitching.

The peaks at (1), (3) and (5) actually occur at the moment where the pitch rate is the highest. With a high pitch or roll rate, a tiny misalignment in time between OptiTrack and the helicopter can cause large errors in the angles. That is exactly what is happening here. The oscillator on the Lisa/S is not as accurate as the one used to log OptiTrack data. The clocks have drifted slightly since the beginning of the log. This means that the actual pitch error at these points is even smaller.

The same phenomena occurs at points (2) and (4), while the helicopter pitches forward to accelerate in the direction of the next waypoint. During the forward acceleration, the pitch error diverges by approximately two degrees, which is considered acceptable. The deceleration which follows helps the estimation error to return to the original value. Larger errors can be expected for longer periods of acceleration.

The error in roll seems to be related to the heading. The roll estimate error is smaller in the sections where the helicopter flies from (A) to (B), compared to when it flies from (B) to (A). This is true for all 12 cycles in the experiment. Also in static conditions, when the helicopter was placed on the ground, the roll angle showed a difference of 1.5° between the two headings used in the flight plan. The pitch angle was also affected by the heading, but had approximately the same value at both headings. The differences are most likely caused by misalignment of the flight arena. The calibration tool for the ground plane turned out to be deformed.

Besides the effects of the misaligned ground-'truth', the roll error appears to be very similar with the hover experiment. Still some small variations occur during maneuvers at (2) and (4). The tail rotor, which causes lateral acceleration, may also affect the roll estimate. The data however shows no clear relation, probably because the lateral acceleration is canceled quickly a the change in the roll angle.

Chapter 2

INDI Derivations

2-1 Closed Loop Input Tracking

The control loop structure of the INDI controller, with actuator dynamics and measurement filters, is shown in Fig. 2-1. The closed loop dynamics of the INDI control loop, which describe the dynamics between the virtual control input $\boldsymbol{\nu}$ and system output $\mathbf{y}_k$, are derived here.

We start by describing small parts of the system:

$$\dot{\mathbf{x}}_m = \mathbf{z}^{-1}\dot{\mathbf{x}}_m + \mathbf{z}^{-1}\mathbf{G}\Delta\mathbf{a} \tag{2-1}$$

$$\left[\mathbf{I} - \mathbf{z}^{-1}\right]\dot{\mathbf{x}}_m = \mathbf{z}^{-1}\mathbf{G}\Delta\mathbf{a} \tag{2-2}$$

$$\Delta\mathbf{a} = \mathbf{A}(z)\left[\mathbf{z}^{-1}\mathbf{G}^{-1}\mathbf{H}(z)\mathbf{G}\Delta\mathbf{a} + \left[\mathbf{I} - \mathbf{z}^{-1}\right]\Delta\mathbf{u}\right] \tag{2-3}$$

$$\left[\mathbf{I} - \mathbf{z}^{-1}\mathbf{A}(z)\mathbf{G}^{-1}\mathbf{H}(z)\mathbf{G}\right]\Delta\mathbf{a} = \mathbf{A}(z)\left[\mathbf{I} - \mathbf{z}^{-1}\right]\Delta\mathbf{u} \tag{2-4}$$

$$\Delta\mathbf{a} = \left[\mathbf{I} - \mathbf{z}^{-1}\mathbf{A}(z)\mathbf{G}^{-1}\mathbf{H}(z)\mathbf{G}\right]^{-1}\mathbf{A}(z)\left[\mathbf{I} - \mathbf{z}^{-1}\right]\Delta\mathbf{u} \tag{2-5}$$

$$\Delta\mathbf{u} = \mathbf{G}^{-1}\left[\boldsymbol{\nu} - \mathbf{H}(z)\dot{\mathbf{x}}_m\right] \tag{2-6}$$

Combining Eq. 2-2, 2-5 and 2-6:

$$\left[\mathbf{I} - \mathbf{z}^{-1}\right]\dot{\mathbf{x}}_m = \mathbf{z}^{-1}\mathbf{G}\left[\mathbf{I} - \mathbf{z}^{-1}\mathbf{A}(z)\mathbf{G}^{-1}\mathbf{H}(z)\mathbf{G}\right]^{-1}\mathbf{A}(z)\left[\mathbf{I} - \mathbf{z}^{-1}\right]\mathbf{G}^{-1}\left[\boldsymbol{\nu} - \mathbf{H}(z)\dot{\mathbf{x}}_m\right] \tag{2-7}$$

$$\dot{\mathbf{x}}_m = \mathbf{z}^{-1}\mathbf{G}\left[\mathbf{I} - \mathbf{z}^{-1}\mathbf{A}(z)\mathbf{G}^{-1}\mathbf{H}(z)\mathbf{G}\right]^{-1}\mathbf{A}(z)\mathbf{G}^{-1}\left[\boldsymbol{\nu} - \mathbf{H}(z)\dot{\mathbf{x}}_m\right] \tag{2-8}$$

$$\left[\mathbf{I} - \mathbf{z}^{-1}\mathbf{A}(z)\mathbf{G}^{-1}\mathbf{H}(z)\mathbf{G}\right]\mathbf{G}^{-1}\dot{\mathbf{x}}_m = \mathbf{z}^{-1}\mathbf{A}(z)\mathbf{G}^{-1}\left[\boldsymbol{\nu} - \mathbf{H}(z)\dot{\mathbf{x}}_m\right] \tag{2-9}$$

$$\mathbf{G}^{-1}\dot{\mathbf{x}}_m = \mathbf{z}^{-1}\mathbf{A}(z)\mathbf{G}^{-1}\boldsymbol{\nu} \tag{2-10}$$

And finally:

$$\dot{\mathbf{x}}_m = \mathbf{z}^{-1}\mathbf{G}\mathbf{A}(z)\mathbf{G}^{-1}\boldsymbol{\nu} \tag{2-11}$$

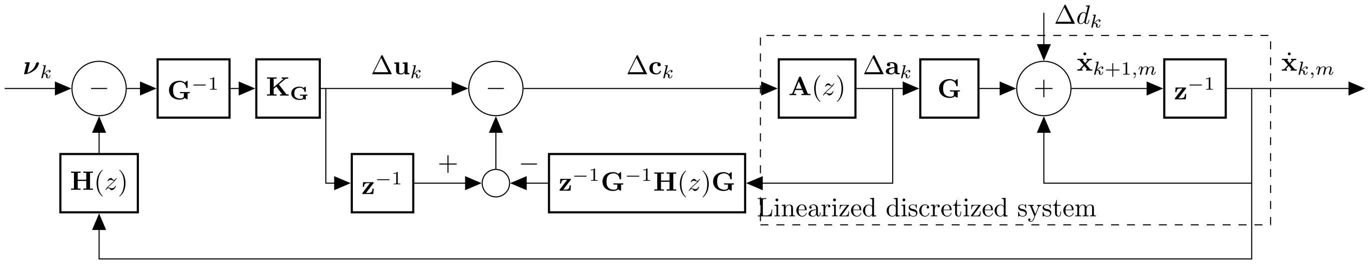

Figure 2-1: INDI block diagram for a discretized linearized system actuator dynamics $\mathbf{A}(z)$, a measurement filter $\mathbf{H}(z)$, a control effectiveness $\mathbf{G}$ and control effectiveness error scalar $\mathbf{K}_G$.

2-2 Control Effectiveness Mismatch

If $\mathbf{K}_G \neq \mathbf{I}$, Eq. 2-6 changes to:

$$\Delta\mathbf{u} = \mathbf{K}_G\mathbf{G}^{-1}\left[\boldsymbol{\nu} - \mathbf{H}(z)\dot{\mathbf{x}}_m\right] \tag{2-12}$$

Substituting in Eq. 2-5 and 2-2 gives:

$$\dot{\mathbf{x}}_m = \mathbf{z}^{-1}\mathbf{G}\left[\mathbf{I} - \mathbf{z}^{-1}\mathbf{A}(z)\mathbf{G}^{-1}\mathbf{H}(z)\mathbf{G}\right]^{-1}\mathbf{A}(z)\mathbf{K}_G\mathbf{G}^{-1}\left[\boldsymbol{\nu} - \mathbf{H}(z)\dot{\mathbf{x}}_m\right] \tag{2-13}$$

$$\left[\mathbf{I} - \mathbf{z}^{-1}\mathbf{A}(z)\mathbf{G}^{-1}\mathbf{H}(z)\mathbf{G}\right]\mathbf{G}^{-1}\dot{\mathbf{x}}_m = \mathbf{z}^{-1}\mathbf{A}(z)\mathbf{K}_G\mathbf{G}^{-1}\left[\boldsymbol{\nu} - \mathbf{H}(z)\dot{\mathbf{x}}_m\right] \tag{2-14}$$

This can be simplified further when considering only a single degree of freedom:

$$\left[1 - z^{-1}A(z)H(z)\right]\dot{x}_m = z^{-1}A(z)K_G\left[\nu - H(z)\dot{x}_m\right] \tag{2-15}$$

$$\left[1 - z^{-1}A(z)H(z) + z^{-1}K_GA(z)H(z)\right]\dot{x}_m = z^{-1}A(z)K_G\nu \tag{2-16}$$

$$\left[1 + z^{-1}A(z)H(z)\left(K_G - 1\right)\right]\dot{x}_m = z^{-1}A(z)K_G\nu \tag{2-17}$$

The transfer function becomes:

$$\dot{x}_m = \frac{A(z)K_G}{z + A(z)H(z)\left(K_G - 1\right)}\nu \tag{2-18}$$

If there is no actuator and no measurement filter, then $A(z) = H(z) = 1$:

$$\dot{x}_m = \frac{K_G}{z + K_G - 1}\nu \tag{2-19}$$

The pole is found by setting the denominator to zero:

$$z + K_G - 1 = 0 \tag{2-20}$$

$$z = 1 - K_G \tag{2-21}$$

Which is in the unit circle for $0 \leq K_G \leq 2$.

A similar derivation is possible without neglecting the actuator. It is shown here for a first-order actuator:

$$A(z) = \frac{z\beta}{z - 1 + \beta} \tag{2-22}$$

where $0 < \beta < 1$. Then, Eq. 2-18 becomes:

$$\dot{x}_m = \frac{\frac{z\beta}{z-1+\beta}K_G}{z + (K_G - 1)\frac{z\beta}{z-1+\beta}}\nu \tag{2-23}$$

$$\dot{x}_m = \frac{\beta K_G}{z - 1 + \beta + (K_G - 1)\beta}\nu \tag{2-24}$$

$$\dot{x}_m = \frac{\beta K_G}{z - 1 + K_G\beta}\nu \tag{2-25}$$

which has a pole at $p = 1 - K_G\beta$. For stability it is required that $0 \leq K_G\beta \leq 1$.

2-3 Disturbance Rejection

When looking at the disturbance rejection response, Eq. 2-1 is extended with a disturbance input $\Delta\mathbf{d}$:

$$\dot{\mathbf{x}}_m = \mathbf{z}^{-1}\dot{\mathbf{x}}_m + \mathbf{z}^{-1}\mathbf{G}\Delta\mathbf{a} + \mathbf{z}^{-1}\Delta\mathbf{d} \tag{2-26}$$

Substituting Eq. 2-5 and 2-6 into Eq. 2-26:

$$\begin{aligned}\left[\mathbf{I} - \mathbf{z}^{-1}\right]\dot{\mathbf{x}}_m = \mathbf{z}^{-1}\mathbf{G}\left[\mathbf{I} - \mathbf{z}^{-1}\mathbf{A}(z)\mathbf{G}^{-1}\mathbf{H}(z)\mathbf{G}\right]^{-1}\mathbf{A}(z)\left[\mathbf{I} - \mathbf{z}^{-1}\right]\mathbf{G}^{-1}\left[\boldsymbol{\nu} - \mathbf{H}(z)\dot{\mathbf{x}}_m\right] \\ + \mathbf{z}^{-1}\Delta\mathbf{d}\end{aligned} \tag{2-27}$$

The increment in disturbance is a function of the full disturbance:

$$\Delta\mathbf{d}_k = \mathbf{d}_k - \mathbf{d}_{k-1} \tag{2-28}$$

Or in z-domain:

$$\Delta\mathbf{d} = \left[\mathbf{I} - \mathbf{z}^{-1}\right]\mathbf{d} \tag{2-29}$$

Substituting Eq. 2-29 in 2-27:

$$\begin{aligned}\left[\mathbf{I} - \mathbf{z}^{-1}\right]\dot{\mathbf{x}}_m = \mathbf{z}^{-1}\mathbf{G}\left[\mathbf{I} - \mathbf{z}^{-1}\mathbf{A}(z)\mathbf{G}^{-1}\mathbf{H}(z)\mathbf{G}\right]^{-1}\mathbf{A}(z)\left[\mathbf{I} - \mathbf{z}^{-1}\right]\mathbf{G}^{-1}\left[\boldsymbol{\nu} - \mathbf{H}(z)\dot{\mathbf{x}}_m\right] \\ + \mathbf{z}^{-1}\left[\mathbf{I} - \mathbf{z}^{-1}\right]\mathbf{d}\end{aligned} \tag{2-30}$$

Which can be reduced to:

$$\dot{\mathbf{x}}_m = \mathbf{z}^{-1}\mathbf{G}\left[\mathbf{I} - \mathbf{z}^{-1}\mathbf{A}(z)\mathbf{G}^{-1}\mathbf{H}(z)\mathbf{G}\right]^{-1}\mathbf{A}(z)\mathbf{G}^{-1}\left[\boldsymbol{\nu} - \mathbf{H}(z)\dot{\mathbf{x}}_m\right] + \mathbf{z}^{-1}\mathbf{d} \tag{2-31}$$

Since we are considering disturbance rejection, $\boldsymbol{\nu}$ is set to zero:

$$\begin{aligned}\left[\mathbf{I} - \mathbf{z}^{-1}\mathbf{A}(z)\mathbf{G}^{-1}\mathbf{H}(z)\mathbf{G}\right]\mathbf{G}^{-1}\dot{\mathbf{x}}_m = &- \mathbf{z}^{-1}\mathbf{A}(z)\mathbf{G}^{-1}\mathbf{H}(z)\dot{\mathbf{x}}_m \\ &+ \mathbf{z}^{-1}\left[\mathbf{I} - \mathbf{z}^{-1}\mathbf{A}(z)\mathbf{G}^{-1}\mathbf{H}(z)\mathbf{G}\right]\mathbf{G}^{-1}\mathbf{d}\end{aligned} \tag{2-32}$$

$$\mathbf{G}^{-1}\dot{\mathbf{x}}_m = \mathbf{z}^{-1}\left[\mathbf{I} - \mathbf{z}^{-1}\mathbf{A}(z)\mathbf{G}^{-1}\mathbf{H}(z)\mathbf{G}\right]\mathbf{G}^{-1}\mathbf{d} \tag{2-33}$$

$$\dot{\mathbf{x}}_m = \mathbf{z}^{-1}\left[\mathbf{I} - \mathbf{z}^{-1}\mathbf{G}\mathbf{A}(z)\mathbf{G}^{-1}\mathbf{H}(z)\right]\mathbf{d} \tag{2-34}$$

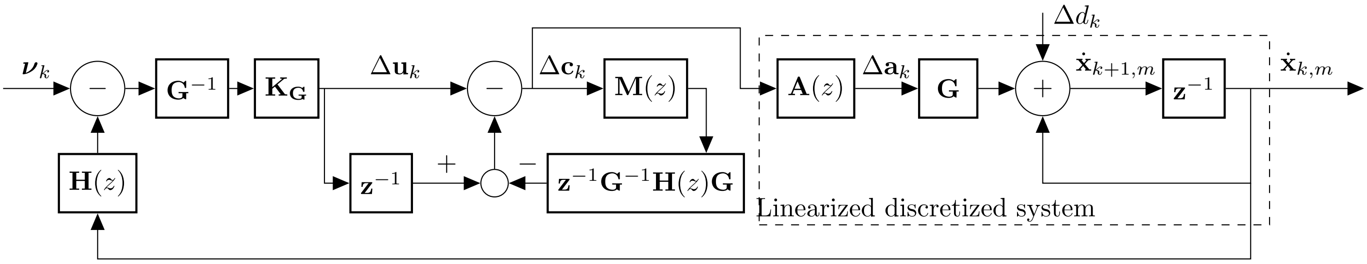

Figure 2-2: INDI block diagram for a discretized linearized system actuator dynamics $\mathbf{A}(z)$, an actuator model $\mathbf{M}(z)$, a measurement filter $\mathbf{H}(z)$, a control effectiveness $\mathbf{G}$ and control effectiveness error scalar $\mathbf{K}_G$.

2-4 Actuator Model Mismatch

Figure 2-2 shows the block diagram of the same INDI loop as in Fig. 2-1, but with an actuator model instead of direct actuator feedback. This section explores the effect of an incorrect actuator model in a single degree of freedom, where the incorrect model is given by:

$$M(z) = \frac{zK_A\beta}{z-1+K_A\beta} \tag{2-35}$$

Both the model and the actual dynamics have a steady-state gain of 1. The actual actuator dynamics are:

$$A(z) = \frac{z\beta}{z-1+\beta} \tag{2-36}$$

The derivation of the closed-loop response to an input is derived for a system with no measurement filter, such that $\mathbf{H}(z) = \mathbf{I}$. Also the actuator effectiveness matrix $\mathbf{G}$ is assumed to be error free, which means $\mathbf{K}_G = \mathbf{I}$. The expression for the actuator increment is given by:

$$\Delta a = A(z)\Delta c \tag{2-37}$$

$$\Delta c = \left[1 - z^{-1}\right]\Delta u + z^{-1}M(z)\Delta c \tag{2-38}$$

$$\left[1 - z^{-1}M(z)\right]\Delta c = \left[1 - z^{-1}\right]\Delta u \tag{2-39}$$

$$\Delta c = \left[1 - z^{-1}M(z)\right]^{-1}\left[1 - z^{-1}\right]G^{-1}\left[\nu - \dot{x}_m\right] \tag{2-40}$$

$$\Delta a = A(z)\left[1 - z^{-1}M(z)\right]^{-1}\left[1 - z^{-1}\right]G^{-1}\left[\nu - \dot{x}_m\right] \tag{2-41}$$

Substituting in Eq. 2-2:

$$\left[1 - z^{-1}\right]\dot{x}_m = z^{-1}GA(z)\left[1 - z^{-1}M(z)\right]^{-1}\left[1 - z^{-1}\right]G^{-1}\left[\nu - \dot{x}_m\right] \tag{2-42}$$

$$\dot{x}_m = z^{-1}A(z)\left[1 - z^{-1}M(z)\right]^{-1}\left[\nu - \dot{x}_m\right] \tag{2-43}$$

$$\left[1 - z^{-1}M(z)\right]\dot{x}_m = z^{-1}A(z)\left[\nu - \dot{x}_m\right] \tag{2-44}$$

$$\left[1 - z^{-1}M(z) + z^{-1}A(z)\right]\dot{x}_m = z^{-1}A(z)\nu \tag{2-45}$$

$$\left[1 - z^{-1}M(z) + z^{-1}A(z)\right]\dot{x}_m = z^{-1}A(z)\nu \tag{2-46}$$

$$\dot{x}_m = \frac{A(z)}{z - M(z) + A(z)}\nu \tag{2-47}$$

Now by substituting Eq. 2-35 and 2-36:

$$\dot{x}_m = \frac{\frac{z\beta}{z-1+\beta}}{z - \frac{zK_A\beta}{z-1+K_A\beta} + \frac{z\beta}{z-1+\beta}}\nu \tag{2-48}$$

$$\dot{x}_m = \frac{z\beta}{z(z-1+\beta) - \frac{zK_A\beta}{z-1+K_A\beta}(z-1+\beta) + z\beta}\nu \tag{2-49}$$

$$\dot{x}_m = \frac{z\beta(z-1+K_A\beta)}{z(z-1+\beta)(z-1+K_A\beta) - zK_A\beta(z-1+\beta) + z\beta(z-1+K_A\beta)}\nu \tag{2-50}$$

$$\dot{x}_m = \frac{\beta(z-1+K_A\beta)}{(z-1+\beta)(z-1+K_A\beta) - K_A\beta(z-1+\beta) + \beta(z-1+K_A\beta)}\nu \tag{2-51}$$

$$\dot{x}_m = \frac{z\beta - \beta + K_A\beta^2}{z^2 + z(2\beta-2) + 1 - 2\beta + K_A\beta^2}\nu \tag{2-52}$$

The roots of the characteristic equation are found at:

$$z^2 + z(2\beta-2) + 1 - 2\beta + K_A\beta^2 = 0 \tag{2-53}$$

$$z = \frac{1}{2}\left(2 - 2\beta \pm \sqrt{4\beta^2 - 8\beta + 4 - 4(1 - 2\beta + K_A\beta^2)}\right) \tag{2-54}$$

$$z = 1 - \beta \pm \sqrt{\beta^2 - K_A\beta^2} \tag{2-55}$$

From this equation, it can be observed that the poles get an imaginary component if $K_A > 1$. To guarantee stability, we have to make sure that the poles are inside the unit circle. This is true for all possible values $0 \leq K_A \leq (1/\beta)$.

Part III

Literature Study

Chapter 3

Introduction

The Unmanned Aerial Vehicle (UAV) business has been a fast-growing market in recent years. UAVs come in many different shapes and sizes and are used in a wide range of applications. The multi-rotor concept is the most common type, since it has several good characteristics. It is capable of Vertical Takeoff and Landing (VTOL). The design is mechanically simple and robust, since the motors are the only moving parts. The maneuverability is generally very good. With a properly tuned attitude controller it is also relatively easy to fly. By including an on-board GPS receiver, it is even possible to fly completely autonomous. All these characteristics make it a very popular platform for hobbyists and professionals.

The downside of the multi-rotor concept is efficiency. A set of smaller rotors is less efficient than a single large rotor that delivers the same amount of thrust Driessens & Pounds (2013). This is exactly what the classical helicopter design looks like. Even with a tail-rotor to compensate for torque of the main rotor, it is more energy efficient. This energy efficiency is a trade-off with robustness. The mechanical design of a helicopter is more complex with servo actuators and a swash-plate mechanism. The design of an attitude controller is more complicated because several cross-coupling effects have to be taken into account.

Nowadays, small RC helicopters toys of decent quality are available. Together with developments in small scale electronics, it is time to reconsider the traditional helicopter configuration for autonomous UAVs. The Walkera Genius CP V2 for example is a light-weight helicopter weighing only 35 grams without battery. Most parts are made out of plastic which can absorb energy in a crash, making it more robust. There are some research projects on autonomous helicopters H. J. Kim et al. (2004); Bing et al. (2012), but these helicopters are much larger. Prox Dynamics has developed the PD-100 Black Hornet, which is a miniature helicopter for military applications, but no details are available on its capabilities and inner workings. As far as is known to the author, no scientific research exists on small-scale ($<$50 gram) autonomous helicopters.

One of the difficulties with (small) helicopters, but also with other small-scale UAVs, is attitude estimation. Without a good attitude estimate, it is impossible to control the attitude. Without attitude control, it is impossible to fly autonomously. Helicopters in particular are known for their strong vibrations. These vibrations are sensed by the accelerometers and can negatively affect the attitude estimation process. On most UAVs, the vibrations are filtered by a mechanical suspension of the sensors using dampers. On a small-scale helicopter however, possibilities for mechanical damping are limited because of the size. Additionally, the choice of inertial sensors is limited to the very small ones, which generally provide lower quality measurements.

The other challenging part is control. The most common approach is to use PID controllers on the attitude angles. Implementation is straightforward, but tuning the gains can be difficult. INDI is a sensor-based control method. Using sensor measurements, the system is feedback linearized and a simple linear controller can be added to control the attitude. Once the actuator effectiveness in the INDI loop has been identified, which can be done automatically by an adaptive algorithm, the UAV shows excellent flight characteristics. This technique was recently implemented on quadcopters with impressive results Smeur et al. (2015). Unfortunately, the same method cannot be directly applied to helicopters. The control effectiveness functions for helicopters are much more complicated Simplicio et al. (2013), which significantly reduces the simplicity of the controller.

3-1 Research questions

The goal of this project is to make a small helicopter fly autonomously outside using INDI. The research is focused at two different topics: attitude estimation and INDI control. The relation between the two is the need to have an attitude estimate in order to control it with INDI. Therefore, two main research questions and their corresponding sub-questions are formulated.

3-1-1 Attitude estimation

The first main research question is:

Can attitude estimation be accomplished with small inertial sensors by using an existing algorithm in combination with vibration attenuation?

This preliminary thesis aims to answer the following subquestions:

- What are the characteristics of small inertial sensors?
- What attitude estimation algorithms exist in literature?
- What would be a suitable attitude estimation algorithm that can be used on a small-scale helicopter?
- What are the options for attenuating vibrations in inertial measurements?

3-1-2 Helicopter INDI control

The second main research question is:

Can INDI be applied directly for rate control of a helicopter UAV?

This preliminary thesis aims to answer the following subquestions:

- What are the control dynamics of a helicopter?
- Is it possible to implement control dynamics as actuator dynamics?

3-2 Layout

Chapter 4 describes the test platform used for this research and the properties of small inertial sensors. The basic concept and two algorithms for attitude estimation are described in Chapter 5. This chapter also describes methods for vibration attenuation which are required for good attitude estimation. The basics of helicopter dynamics and existing controllers are described in Chapter 6. Chapter 7 explains the concept of INDI and how it can be applied for helicopter control. The project planning is given in Chapter 8 and the conclusions can be found in Chapter 9.

Chapter 4

Test Equipment

This chapter describes the helicopter that is used for this project, including modifications. The last section describes the working principles of Micro-Electrical-Mechanical system (MEMS) inertial sensors, which are typically used on small UAVs.

4-1 Helicopter

The helicopter used for this research project is the Walkera Genius CP V2 and is shown in Figure 4-1. Without modifications and without battery, it weighs only 35 grams. Unlike most other toy helicopters in this class, the Walkera Genius CP V2 does not have a flybar for stabilization. It has built-in accelerometers and gyroscopes to stabilize attitude.

Specifications of the Walkera Genius CP V2:

- Main rotor diameter: 240 mm
- Tail rotor diameter: 45 mm
- Overall length: 220 mm
- Weight: 35 g
- Battery: 3.7V 200 mAh Li-Po

4-2 Brushless upgrade

By default, the helicopter is equipped with a brushed motor which drives main the shaft through gearing. Brushless motors have several advantages over brushed motors, including higher efficiency, less maintenance and better heat dissipation. Walkera offers a brushless

Figure 4-1: Walkera Genius CP V2 unmodified.

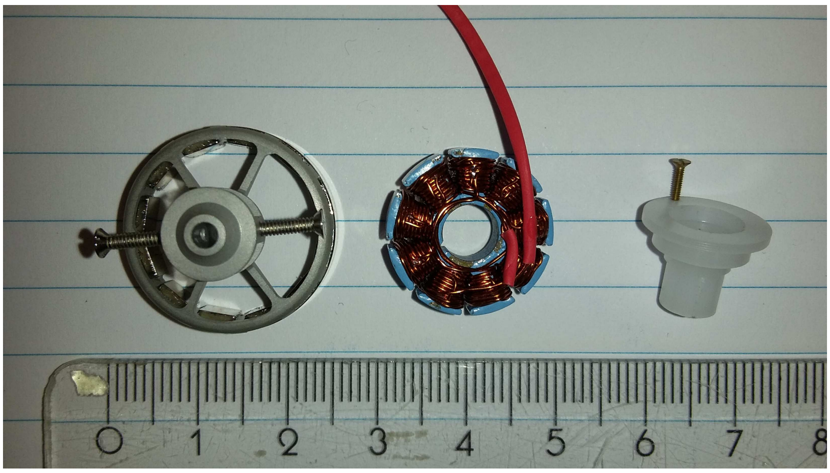

Figure 4-2: Glavak brushless direct drive motor and adapter piece.

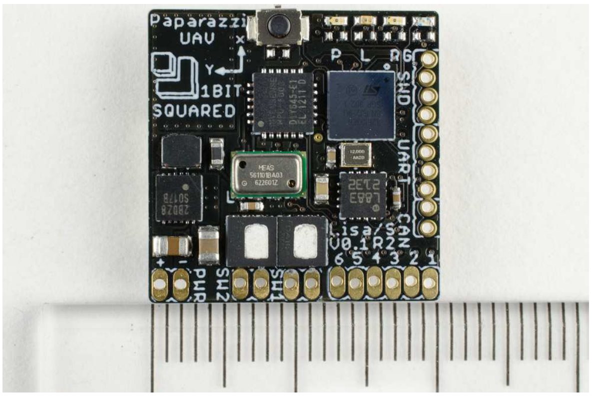

Figure 4-3: Lisa/S autopilot.

upgrade kit to replace the brushed motor. With this upgrade kit, the gearing still remains. The plastic gears wear out quickly and are an extra source of vibrations.

Therefore, the helicopter is upgraded with a direct-drive brushless motor from Glavak. An adapter piece is made from nylon to attach the motor to the helicopter frame. A longer drive shaft is required to extend into the new motor. Figure 4-2 shows a picture of the stator and rotor of the Glavak motor and the nylon adapter piece.

4-3 Autopilot

For research purposes, it is necessary to be able to write custom control software. Therefore, the electronics board which provides the radio link and stabilization, is removed. It is replaced by the Lisa/S autopilot Remes et al. (2014) which was developed by the research group at the MAVLab and is shown in Figure 4-3. The data link is not fast enough to transmit accelerometer and gyroscope measurements real-time. A 4GB micro-SD card is soldered directly to the Lisa/S autopilot to store measurement data which can be retrieved later when the measurement has finished. Telemetry is done through an ESP-8266 WiFi chip. For the radio communication link, a DSM2 deltang receiver is used.

Specifications of the Lisa/S autopilot:

- Size: 2.0 x 2.0 x 0.5 cm
- Weight: 2.8 g
- Processor: 72MHz 32bit ARM Cortex M3 MCU with 16KB RAM and 512KB Flash
- IMU: InvenSense MPU-6050 3-axis gyroscope and 3-axis accelerometer
- Magnetometer: HMC5883L
- Barometer: MS5611
- GPS: ublox MAX-6 series

4-4 MEMS gyroscopes and accelerometers

There are many kinds of sensors to measure acceleration and angular velocity. However, UAVs are forced to use small and light-weight devices. MEMS sensors are the most common type of sensors found on UAVs.

The Lisa/S has an MPU-6050 from Invensense, which is a small chip that contains a 3-axis MEMS gyroscope and 3-axis MEMS accelerometers. This type is similar to those found in smartphones. The chip measures just 4x4x0.9 mm and costs only a few dollars.

4-4-1 Accelerometer measurements

In principle, a MEMS accelerometer consists of a small mass-spring system. Capacitive plates are attached to the proof mass and form capacitors together with fixed plates. When the position of the proof mass changes, it changes the capacitance. The difference in capacitance of two subsequent capacitors are a measure for displacement. Since the position of the proof mass in a mass-spring system relates to the applied force, it can be used to measure acceleration.

Since the accelerometers are used to correct for drift, they should be free of drift themselves. Bias stability Martin et al. (2013) is therefore an import measure. It quantifies the possible variations of the slowly varying static error, which is mainly a result of temperature changes. Temperature variations can degrade performance of a MEMS sensor significantly, so most of these sensors have internal temperature compensation.

Nonlinearity is a parameter which describes the offset from a best fit straight line. The accelerometer based attitude to which the estimation converges can be off due to this effect. Also, sensor noise is usually high with MEMS accelerometers. But since they are used to correct long term drift, high frequency noise is not necessarily a problem. Other types of errors exist as well, but these are smaller and assumed to be negligible.

4-4-2 Gyroscope measurements

The gyroscope sensor in the MPU-6050 consists of a resonating proof mass. Out of plane oscillation due to the Coriolis effect is measured by measuring change in capacitance. This is a direct measure for rotational velocity. Similar to MEMS accelerometers, the MEMS gyroscope is also subject to bias (stability) error, nonlinearity and noise. Most sensor fusion algorithms try to estimate the gyroscope bias using accelerometer measurements. Sensor noise is important since it directly integrates into the attitude estimate. Sensor noise in MEMS gyroscopes is generally low, so the measurements remain useful.

4-4-3 Amplitude and frequency limitations

Accelerometer and gyroscope sensors are only producing valid results when their limitations are not exceeded. Above these limitations, the sensors will still produce data and it will be difficult to see whether it is valid or not.

The sampling rate of the sensor defines the maximum measurable frequency, which is half of that. Any frequency above the Nyquist frequency will appear as a reflections, resulting in false measurements. It is important to prevent high frequency signals from reaching the sensors. This is usually done with physical dampers. Another important frequency that must be prevented from reaching the sensor is the resonance frequency of the proof mass inside the sensor. A recent study Son et al. (2015) showed that it is possible to bring down drones by producing sound at the resonance frequency of the gyroscope sensor.

For both accelerometers and gyroscopes, if the proof mass inside the sensor reaches the maximum deflection, it may start bouncing and even destroy the sensor. This will be the cause of false measurements and should be prevented at all time.

4-4-4 Thermal MEMS accelerometers

A thermal MEMS accelerometer Fennelly et al. (2012) is based on the principle of convection of heated gas. Highly accurate temperature sensors sense the difference throughout the cavity and can thereby sense acceleration. This type of accelerometer has a very low bandwidth and is insensitive to high frequency vibrations. The convection of gas acts as a low-pass filter which also introduces delays. However, since accelerometers are only used to compensate for long-term drift, a thermal MEMS accelerometer may still provide a good solution for attitude estimation in combination with a MEMS gyroscope. The dimensions of these accelerometers are slightly larger compared to regular MEMS accelerometers.

Chapter 5

Attitude Estimation

To achieve autonomous flight, it is essential to have a correct attitude estimate. The attitude is used for control of the thrust vector and thereby the lateral accelerations. If the estimate is wrong, the helicopter will drift from the desired position or flight path. This chapter describes the basic concept behind attitude estimation in Section 5-1. The Kalman filter and Complementary filter are explained respectively in Sections 5-2 and 5-3. Section 5-4 elaborates on vibration attenuation methods to improve attitude estimation.

5-1 Basic concept

The most commonly used methods for attitude estimation on UAVs rely on combined gyroscope and accelerometer measurements. Gyroscopes measure the angular velocities and an attitude estimate is obtained from integration. However, small errors in angular velocity measurement will integrate towards large errors in the attitude estimate. This is compensated with accelerometer measurements. Among other accelerations (and noise), accelerometers measure the direction of the gravity vector. The pitch and roll angle can be derived from the direction of the gravity vector in the body frame. Drift in yaw is usually corrected with magnetometer measurements. Heading estimation on a small helicopter poses no new challenges compared to other UAVs, because magnetometers are not affected by vibrations. Therefore this study only focuses at attitude (pitch and roll) estimation.

$$a_{meas} = a_{grav} + a_{dyn} \tag{5-1}$$

Equation 5-1 shows that the measured acceleration of a perfect sensor is the sum of gravity and dynamic accelerations. Only if the dynamic accelerations are zero, the measured acceleration can be used to obtain the attitude. For the dynamic accelerations to be zero, the aerial vehicle must be moving at a constant velocity. Vibrations in the vehicle are another type of dynamic accelerations and should also be zero for a correct attitude estimate.

These restrictions would basically render accelerometer measurements unusable in practice. But in the long-term, when the average of dynamic accelerations approaches zero, the accelerometers provide a reasonable estimate of the direction of the gravity vector. This long-term estimate is used to compensate long-term drift of gyroscope integration, thereby able to provide a reasonable attitude estimate.

This trick does not work in situations where dynamic accelerations do not average to zero, for example when flying in circles. In that case, it is required to subtract centripetal accelerations, which can only be calculated when velocity is known.

5-2 Kalman filter

The Kalman filter is a very common choice for attitude estimation Carminati et al. (2012); Wang et al. (2004); Suh (2010); Makni et al. (2014); Kang & Park (2009); Gebre-Egziabher et al. (2004); Li & Wang (2013). Pitch and roll angles can be obtained from fusing gyroscope and accelerometer measurements. Magnetometer measurements are commonly included to also obtain heading information.

5-2-1 Linear Kalman filter

The Kalman filter is an algorithm that provides the optimal state estimate of a linear dynamic system by fusing noisy measurement data. The standard discrete-time state-space model is given by:

$$x(t+1) = F \cdot x(t) + v_1(t) \tag{5-2}$$

$$y(t) = H \cdot x(t) + v_2(t) \tag{5-3}$$

These equations are referred to as the process equation and the measurement equation. The F matrix contains system dynamics. H is the model that describes how sensor readings are reflected on the state. v_1 and v_2 are Gaussian noise, where v_1 is the process noise and v_2 describes measurement noise.

Each iteration follows a predictor-corrector feedback mechanism. The *a priori* state estimate is obtained by propagating according to the model in the process equation. The *a posteriori* state estimate then follows from sensor measurements in a correction step.

Table 5-1 contains the most general description of the Kalman filter. There is no single solution for using a Kalman filter for attitude estimation. Different variables can be chosen as states and different variations to the Kalman filter exist.

5-2-2 Attitude representations

There are three common choices for attitude representation: Euler angles Foxlin (1996); Leavitt et al. (2006); Suh (2006), direction cosines Carminati et al. (2012); Lundberg et

Table 5-1: Linear Kalman Filter

0.	Obtain initial state estimate and covariance matrix:	$\hat{x}_{0,0}, P_{0,0}$
	Begin iteration	
1.	One-step ahead prediction	$\hat{\underline{x}}_{(k+1,k)} = \Phi_{(k+1,k)}\hat{\underline{x}}_{(k,k)} + \Psi_{(k+1,k)}\underline{u}_{(k)}$
2.	Covariance matrix of state prediction error	$P_{(k+1,k)} = \Phi_k P_k \Phi_k^T + Q_{(d,k)}$
3.	Calculate Kalman gain	$K_{(k+1)} = P_{k+1,k} H_{(k+1)}^T \left(H_{(k+1)} P_{(k+1)} H_{(k+1)}^T + R_{(k+1)} \right)^{-1}$
4.	Measurement update	$\hat{\underline{x}}_{(k+1,k+1)} = \hat{\underline{x}}_{(k+1,k)} + K_{(k+1)} \left(\underline{z}_{(k+1)} - H_{(k+1)} \hat{\underline{x}}_{(k+1,k)} \right)$
5.	Covariance matrix of state estimation error	$P_{(k+1,k+1)} = \left(I - K_{(k+1)} H_{(k+1)} \right) P_{(k+1,k)}$

al. (2000); Rehbinder & Hu (2001) and quaternions Xiong et al. (2011); Barshan & Durrant-Whyte (1995); S. h. P. Won et al. (2009); S. H. P. Won et al. (2010); Wang et al. (2004); A. Kim & Golnaraghi (2004); Choukroun et al. (2006); Greene & Trent (2003); Bijker & Steyn (2008); Vaganay et al. (1993); Yun et al. (2003); Lee & Park (2009). Using Euler angles is the most intuitive approach, but contains nonlinear equations and suffers from at least one singularity Lee & Park (2009). Direction cosines and quaternions do not have singularities and possess better numerical behavior. Direction cosines are mainly chosen for systems where heading is irrelevant, because it saves one state variable compared to quaternions. Quaternions are a computational friendly and singularity-free solution for full 3D direction information and therefore the most popular choice in an Attitude and Heading Reference System (AHRS).

5-2-3 Direct and Indirect Kalman filter

There are two main designs for a Kalman filter: direct and indirect. With the direct Kalman filter, the state vector contains all the variables of interest. The state vector of an indirect Kalman filter only holds an error-state. This can be the difference in state estimated from gyroscope integration and accelerometer measurements. The advantage of an indirect filter is that the state dimension is smaller and it requires less computations Carminati et al. (2012); Suh (2010). However, with the simplifications in the indirect filter, the achievable performance is lower. It still shows excellent performance with both Euler angles Setoodeh et al. (2004) and quaternions Suh (2010).

5-2-4 External accelerations

As mentioned in section 5-1, accelerometer measurements can not simply be used to detect the gravity vector if external accelerations are present. For some applications like slow-moving airships Bijker & Steyn (2008), it is safe to assume that there are no external accelerations.

Other researchers A. Kim & Golnaraghi (2004); Vaganay et al. (1993) report that their filter is still able to accurately estimate attitude when it is subject to small zero-mean or short-lived external accelerations. No details are provided on the measurement noise covariance matrix R, but it is suspected that this matrix is tuned with higher values than the actual sensor noise. Thereby it is effectively reducing the weights of the accelerometers in the fusion process.

Other researchers have considered the impact of external accelerations on the performance of attitude estimation and proposed methods to improve the fusion algorithm. These methods are based on detection of external acceleration, which can be done by comparing the measurements with gravity. A common method is to use a switching mechanism with thresholds, which reduces the weights of accelerometer measurements when external acceleration is detected Sabatini (2006); Suh et al. (2006); Wang et al. (2004); Li & Wang (2013). By using direction information of external acceleration, unnecessarily lowering weights on accelerometer outputs that are not affected by the acceleration can be prevented, giving better results Suh (2010).

Lee et al. (2012) used a model-based approach to solve the problem. This algorithm was capable of estimating accurate attitudes and external accelerations for short accelerated periods, but showed gradually increasing errors when the testing condition involved prolonged high external accelerations. This works well if it involves wearable sensors, but might not be sufficient for UAV applications.

A more advanced method, the quaternion-based Adaptive Kalman filter (q-AKF), was recently proposed Makni et al. (2014). It continuously estimates the covariance matrix associated with external acceleration. It is based on a method for unknown noise statistics. This method needs no tuning of thresholds and also automatically incorporates directional information as proposed by Suh Suh (2010).

5-3 Complementary filter

The other common choice for attitude estimation is a complementary filter Baerveldt & Klang (1997a); Roberts et al. (2003); Hamel & Mahony (2006). With low-quality inertial sensors such as the MPU-6050 on the Lisa/S, a Kalman filter can be difficult to apply due to the non-linearities and non-Gaussian noise characteristics Mahony et al. (2005); Higgins (1975). A complementary filter provides a good alternative since no assumptions are made about linearity and noise statistics Brown & Hwang (1992). Compared to a Kalman filter, it is mathematically simpler and computationally less expensive.

5-3-1 Basic complementary filter

The basic idea of a complementary filter is to combine measurements of two or more sensors, using only the reliable frequencies of each sensor, to provide a reliable signal over the entire bandwidth. To achieve a reliable attitude estimate, the low-frequency data of the accelerometers can be combined with high-frequency data from gyroscopes in a complementary filter. A block-diagram of a basic complementary filter is shown in Figure 5-1, with the following transfer function: Jensen et al. (2013)

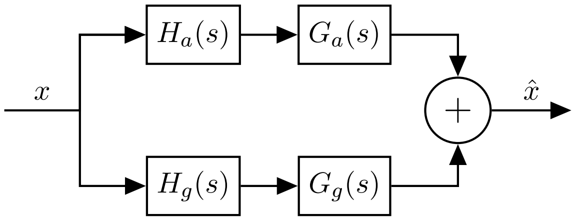

Figure 5-1: Frequency domain complementary filter Jensen et al. (2013).

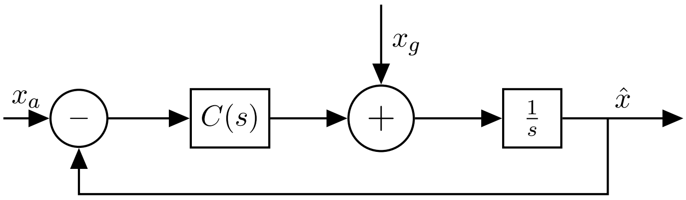

Figure 5-2: Closed-loop complementary filter system Jensen et al. (2013).

$$H_a(s)G_a(s) + H_g(s)G_g(s) = 1 \tag{5-4}$$

H_a and H_g represent the accelerometer and gyroscope sensors. The corresponding filters are G_a and G_g. If the transfer function of the complete system is approximately equal to 1, the output is an estimate for attitude. When the sensor dynamics are not exactly known, an ideal sensor may be assumed ($H = 1$) while G_a and G_g are set as generic filters that can be tuned to minimize the estimation error Jensen et al. (2013). The assumption of an ideal sensor is also valid if the sensor measurements are only valid in the range of G. For an attitude estimation filter, G_a is configured as a low-pass filter for accelerometers and G_g is a high-pass filter for the gyroscopes.

By choosing G_a and G_g as follows, a classical closed-loop complementary filter can be obtained:

$$G_a(s) = \frac{C(s)}{C(s) + s} \tag{5-5}$$

$$G_g(s) = \frac{s}{C(s) + s} \tag{5-6}$$

The corresponding block diagram is given in Figure 5-2. The simplest complementary filter contains only proportional feedback by $C(s) = k$. The gain k is then the crossover frequency for the filter. If the gyroscope measurements contain a bias term, which is usually the case for MEMS gyroscopes, it is possible to add an integrator term into the compensator:

$$C(s) = k + \frac{1}{\lambda s} \tag{5-7}$$

5-3-2 Direct and passive complementary filter

Mahony et al. (2005) proposed two non-linear filters: the direct and passive complementary filter. Although these filters were already used before, they were never classified as such and their publication provides the mathematics behind these filters.

The filters are constructed in special orthogonal group denoted SO(3). The following frames of reference are used

- $\mathcal{A}$ denotes the inertial frame of reference.
- $\mathcal{B}$ denotes the body-fixed frame of reference.
- $\mathcal{E}$ denotes the estimator frame of reference.

The system considered is the kinematics of the orientation matrix R:

$$\dot{R} = R\Omega_\times \tag{5-8}$$

where R is the rotation matrix from inertial frame $\mathcal{A}$ to body fixed frame $\mathcal{B}$. Ω is the vector with rotational rates in body-fixed frame. $\Omega_\times$ is the skew-symmetric matrix such that $\Omega_\times v = \Omega \times v$. The dynamics of the direct and passive complementary filter are proposed as: Mahony et al. (2005, 2008)

$$\dot{\hat{R}}_d = \left(R_y\Omega + k_P\hat{R}_d\omega\right)_\times \hat{R}_d = \hat{R}_d\left(\tilde{R}_d\Omega + k_P\omega\right)_\times \tag{5-9}$$

$$\dot{\hat{R}}_p = \left(R_p\Omega + k_P\hat{R}_p\omega\right)_\times \hat{R}_p = \hat{R}_p\left(\Omega + k_P\omega\right)_\times \tag{5-10}$$

where $\hat{R}_d$ and $\hat{R}_p$ denote the estimate of the rotation matrix R using the direct and passive non-linear complementary filter. R_y is an estimate of the rotation matrix based *directly* on accelerometer and magnetometer measurements, hence the name direct complementary filter. The error matrix $\tilde{R}_d = \hat{R}_d^T R_y$ (reps. $\tilde{R}_p = \hat{R}_p^T R_y$) is a noisy measurement of the attitude of the body fixed frame $\mathcal{B}$ with respect to the estimator frame $\mathcal{E}$. The innovation term ω is chosen as $\omega = \mathbb{P}_a(\tilde{R})$, where $\mathbb{P}_a$ is the anti-symmetric projection operator such that $\mathbb{P}_a(\tilde{R}) = \frac{1}{2}\left(\tilde{R} - \tilde{R}^T\right)$. k_P is a positive gain.

Figures 5-3 and 5-4 show the block diagrams of both filters. The main difference between the direct and passive complementary filter is which rotation matrix is used for propagation of gyroscope measurements. The direct filter uses R_y, which is very noisy because it directly uses accelerometer and magnetometer measurements. This noise will propagate further since the gyroscope measurements are integrated in this estimate. The passive filter uses $\hat{R}$ in a feedback structure and is less sensitive to this noise.

Both filters can also be extended with a bias estimator, to correct for bias in the gyroscopes. The measured values from gyroscope measurements are then denoted by

$$\Omega_y = \Omega + b \tag{5-11}$$

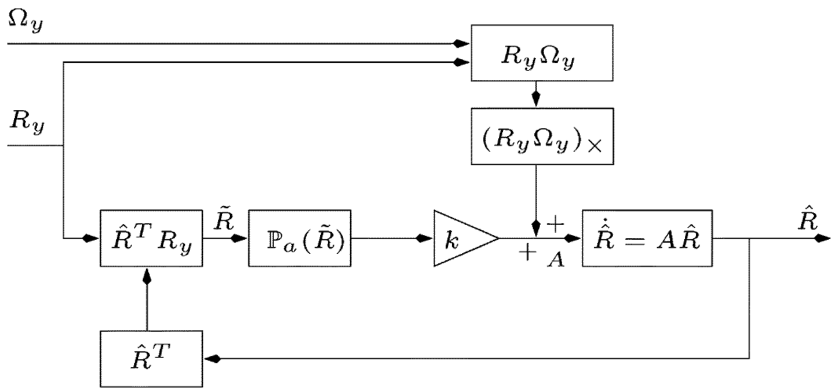

Figure 5-3: Block diagram of the direct complementary filter on SO(3) Mahony et al. (2008).

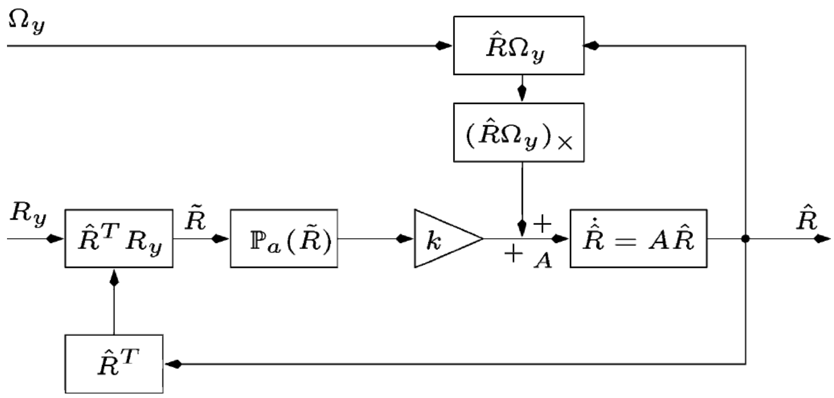

Figure 5-4: Block diagram of the passive complementary filter on SO(3) Mahony et al. (2008).

where b is a constant or slowly varying bias. The *direct complementary filter with bias compensation* is then defined by Mahony et al. (2008) as:

$$\dot{\hat{R}}_d = \left(R_y\left(\Omega_y - \hat{b}\right) + k_P \hat{R}_d \omega\right)_\times \hat{R}_d \tag{5-12}$$

$$\dot{\hat{b}} = -k_I \omega \tag{5-13}$$

$$\omega = \text{vex}\left(\mathbb{P}_a\left(\tilde{R}_d\right)\right) \tag{5-14}$$

The vex operator returns vector v from the skew-symmetric matrix, such that $v = \text{vex}(v_\times)$. The *passive complementary filter with bias compensation* is given by: Mahony et al. (2008)

$$\dot{\hat{R}}_p = \hat{R}_p\left(\Omega_y - \hat{b} + k_P \omega\right)_\times \tag{5-15}$$

$$\dot{\hat{b}} = -k_I \omega \tag{5-16}$$

$$\omega = \text{vex}\left(\mathbb{P}_a\left(\tilde{R}_p\right)\right) \tag{5-17}$$

5-3-3 Explicit complementary filter

After the direct and passive complementary filter, the explicit complementary filter was proposed by Mahony et al. (2008). This is a further development on the passive complementary filter that provides a formulation in terms of measurement error to avoid algebraic reconstruction of the attitude. It requires only accelerometer and gyroscope measurements and gyro biases are also estimated. The explicit complementary filter with bias compensation is formulated as

$$\dot{\hat{R}}_e = \hat{R}_e\left(\left(\Omega_y - \hat{b}\right)_\times + k_P\left(\omega_{mes}\right)_\times\right) \tag{5-18}$$

$$\dot{\hat{b}} = -k_I \omega_{mes} \tag{5-19}$$

$$\omega_{mes} := \sum_{i=1}^{n} k_i v_i \times \hat{v}_i \tag{5-20}$$

where v_i denotes a set of n known inertial directions (gravity, magnetic field) and k_i are the corresponding gains. This algorithm also remains well conditioned in the case where only a single vector direction is measured. The algorithm is also suitable for efficient implementation using the quaternion representation.

5-3-4 External accelerations

A complementary filter has similar issues with external accelerations as a Kalman filter. Several techniques have been developed for the Kalman filter and are described in Section 5-2-4. This is not the case for complementary filters. Many authors Gebre-Egziabher et al. (1998);

Euston et al. (2008); Baerveldt & Klang (1997a,b) use the assumption that low-frequency measurements of the accelerometer represents gravity. This assumption works out well if the gains are properly tuned and the amount of dynamic accelerations is limited. Still, the threshold switching methods that have been applied in combination with Kalman filters would also be applicable to complementary filters. Instead of varying the measurement covariance matrix, the cross-over frequency of the complementary filter can be changed dynamically.

5-4 Vibration attenuation methods

Section 5-2-4 and 5-3-4 already refer to the problem of dynamic accelerations which are picked up by the accelerometer. This section deals with a special kind of dynamic accelerations: vibrations. Literature often refers to motor vibrations as noise. However, the accelerations caused by vibrations are true accelerations and should not be classified as noise. To improve state estimation, these vibrational accelerations should be removed from the accelerometer measurements.

5-4-1 Mechanical damping

First of all, vibrations should be reduced mechanically. Almost any UAV has dampers to separate the inertial sensors and battery from the main body. By including the battery, the mass of the suspended system is increased which provides better damping of high frequency vibrations. The main purpose of mechanical damping is to prevent signals that are outside the measurements range from reaching the sensors.

5-4-2 Software filtering

Several methods can be considered to remove vibrations from accelerometer measurements. The strongest vibrations are introduced by the main motor and rotor. The frequency is known from an RPM sensor which is attached to the motor phases. If an RPM sensor is not available, a real-time Fourier transform can be used to identify vibration frequencies. Using a notch filter it is possible to remove a small bandwidth around the rotor frequency. A notch filter was successfully applied by C. Kim et al. (2012) to enhance state estimation. However, their publication does not go into detail on how the Kalman filter fuses this information and how the measurement covariance matrix is tuned.

In this preliminary study, strong vibrations are measured at the rotor frequency (at 60 Hz) and its harmonics. It is suspected that the first harmonic is caused by aerodynamics from the two rotor blades. The other harmonics remain unexplained, but their amplitude is also much lower. Three notch filters at the rotor frequency and the first harmonics remove the largest vibrations. Figure 5-5 shows the original and resulting signal of lateral accelerations in the helicopter during motion. The motion was generated by a person shaking the helicopter while the main rotor was spinning. It does not yet prove that the filters work for state estimation, but it does show that the strong oscillation can be removed.

Another option is to use a low-pass filter. A first-order low-pass filter is already implemented in the complementary filter in the paparazzi autopilot software, but the main vibration of the

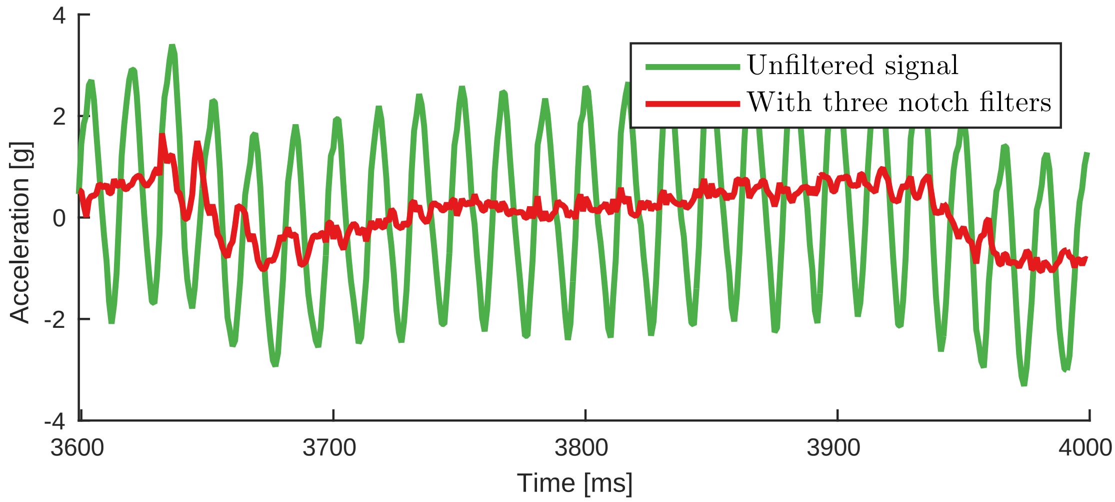

Figure 5-5: Vibration attenuation of the main rotor frequency and harmonics using three notch filters.

helicopter has a relatively low frequency and is not sufficiently attenuated by this filter. Other higher order low-pass filters exist with better delay characteristics and stronger attenuation beyond the cut-off frequency. A combination of notch filters and a low-pass filter can give even better results, although this also introduces delays. Due to causality, delay is inevitable with online low-pass filters. Zero delay can only be achieved by including future measurements.

Chapter 6

Helicopter Dynamics and Control

A helicopter has four control inputs: Three for the main rotor and one for the tail rotor. The rotational speed of the main rotor is approximately constant. A non-linear helicopter model is described in the first section. Section 6-2 describes differences between different types of rotors. Section 6-3 describes dynamics of a rigid spinning disc, which provides some insights in control of gyroscopes. This is useful because the main rotor is basically a giant gyroscope. The final section describes control methods that have been successful in helicopter control.

6-1 Helicopter Model

Previous work by Simplicio et al. (2013) on INDI for helicopter control was based on a non-linear 8-Degrees Of Freedom (DOF) helicopter model. The work studies a full size Bölkow Bö-185 helicopter. The helicopter used in the current project is multiple orders of magnitude smaller and lighter. Size and weight are both parameters of the model. It is expected, but not proven, that the same model can be applied for the smaller helicopter by changing the set of parameters.

The model has 8 degrees of freedom. The first six are three rotations and three translations. The latter two contain the dynamic inflows of the main- and tail rotor. Although it has many simplifying assumptions, the model still captures the important non-linearities and cross-couplings between different DOFs. The non-linearities are mainly related to the airspeed of the rotor disc-plane.

Only the steady-state rotor disc-tilt motion is considered in the model. Flapping dynamics are neglected. The disc-tilt angles are described by a set of non-linear equations which contain, among others, the control inputs. The disc-tilt angles are then used to calculate the rotor forces and moments which are acting on the body. The equations for the disc-tilt angles also contain the pitch- and roll rate of the helicopter body. This is an important term which causes damping of the rotation rates.

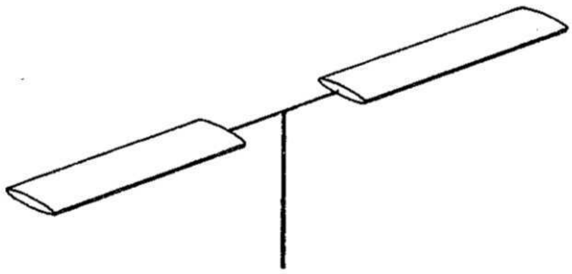

Figure 6-1: Teetering rotor. Padfield (2008)

6-2 Rotor types

Different types of rotors have different dynamics. The different dynamics are described by the 8-DOF helicopter model and can be selected by setting the right parameters. For INDI control, it is fundamental to understand the relation between control inputs and rotational motions.

6-2-1 Teetering rotor

A teetering rotor as in Figure 6-1 has two blades with a central hinge like a seesaw. This type of rotor does not transfer a moment to the rotor shaft. The lift vector is perpendicular to the rotor disc. In hovering flight, the lift vector is aligned with the helicopters center of mass. Tilting the rotor disc causes an offset between the lift vector and the center of mass, thereby inducing rotational acceleration. So in order to control rotational acceleration, the orientation of the rotor disc must be controlled.

The swashplate controls the pitch angle of the rotor blades. By tilting the swashplate, the blade pitch is increased on one side and decreased on the other side. The change in pitch causes a change in lift force and creates a moment around the central hinge. Because of the gyroscopic effect, a rotation is induced on the perpendicular axis. For example, with a counter-clockwise rotating rotor, an increase in pitch on the left side will cause the rotor disc to tilt forward.

6-2-2 Fully articulated rotor

A fully articulated rotor as in Figure 6-2 has a flapping hinge for each blade, allowing the blades to move up and down independently. The blades can also rotate in plane about a lead/lag hinge. The lift vector is perpendicular to the Tip-Path Plane (TPP). In addition, there is a hub moment caused by the offset of the flapping hinges. The offset of the flapping hinge is described as a fraction of the rotor diameter R:

$$e = \frac{r_{\text{hinge}}}{R} \tag{6-1}$$

Due to the hub moment, an articulated rotor has a faster response to a cyclic input compared to a teetering rotor. The rolling response to a cyclic input is given by Bramwell et al. (2000):

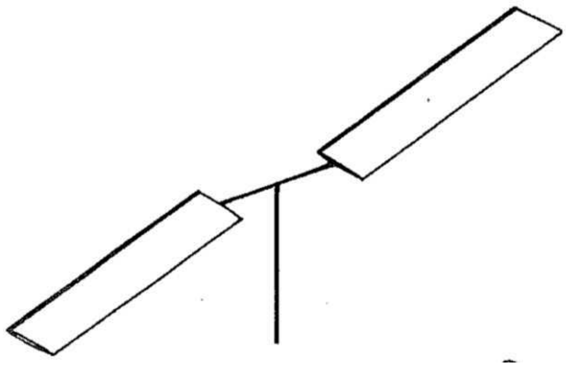

Figure 6-2: Articulated rotor. Padfield (2008)

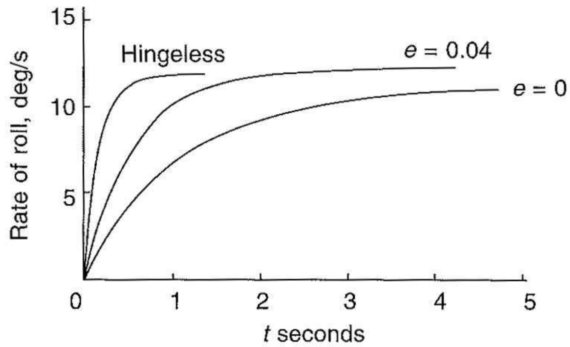

Figure 6-3: Roll rate in response to a step input on the lateral cyclic. Bramwell et al. (2000)

$$\frac{d\phi}{dt} = -\frac{l_{A_1}}{l_p}(1 - e^{l_p t})A_1 \tag{6-2}$$

In this equation, A_1 is the cyclic input, l_{A_1} is a dimensionless representation of control power and l_p is a dimensionless damping term. The damping term increases as a function of the hub moment. Higher hub moments have higher damping an thus result in faster response. Numerical examples for this are given in Figure 6-3. The line $e = 0$ represents a teetering rotor, since this type has no hinge offset and no hub moment.

6-2-3 Hingeless rotor

A hingeless rotor shown in Figure 6-4 is similar to a fully articulated rotor, but instead of hinges it has elastic elements. This is made possible from the increasing understanding of rotor dynamics and aeroelasticity. The hub moment is the largest of all rotor types, and thereby the responsiveness is the highest. This can be seen in Figure 6-3. The Walkera Genius CP V2 helicopter, which is used for this project, has this type of rotor. It is therefore expected that the rotational rates of the Walkera helicopter converge quickly to a steady-state value. The settling times for the different rotors in Figure 6-3 are indicative for full size helicopters. The small model helicopter is expected to have a much smaller ratio between body inertia and rotor moments, which will give an even faster settling time.

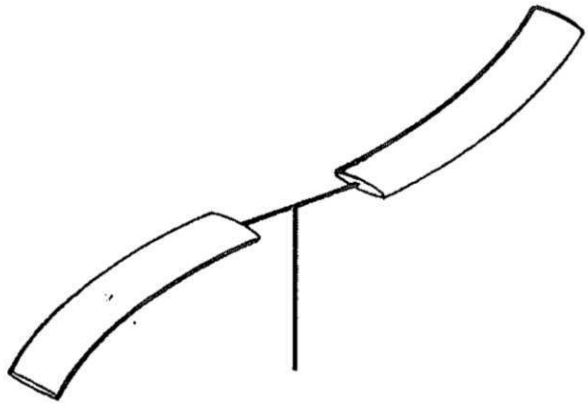

Figure 6-4: Hingeless rotor. Padfield (2008)

6-3 Dynamics of a spinning disc

A rotor is basically a large gyroscope. For a theoretical analysis, it can be described as a rigid spinning disc. Using pure rigid body dynamics, the general equations are:

$$\mathbf{M} = \mathbf{I} \cdot \dot{\omega} + \omega \times (\mathbf{I} \cdot \omega) \tag{6-3}$$

which can be expanded to

$$M_x = I_{xx}\dot{\omega}_x + (I_{zz} - I_{yy})\,\omega_y\omega_z \tag{6-4}$$
$$M_y = I_{yy}\dot{\omega}_y + (I_{xx} - I_{zz})\,\omega_z\omega_x \tag{6-5}$$
$$M_z = I_{zz}\dot{\omega}_z + (I_{yy} - I_{xx})\,\omega_x\omega_y \tag{6-6}$$

$I_{xx} = I_{yy}$ because of symmetry of the disc. ω_z is the rotational speed. If the disc is stationary ($\omega_z = 0$), the applied moments are directly coupled to the rotational accelerations. It will simply accelerate in the direction of moment.

That changes dramatically when $|\omega_z| \gg 0$. When a moment M_x is applied, it will initially accelerate in that direction. This acceleration results in a velocity ω_x, which also appears in the second term of Eq. 6-5. But the applied moment M_y is zero, so $\dot{\omega}_y$ needs to compensate for this. In fact, the Eqs. 6-4 - 6-6 describe a coupled system of differential equations. The differential equations are expressed in the reference frame that is rigidly attached to the spinning disc. It is more convenient to use a reference frame that is attached to the spinning disc, but is not rotating around the spinning axis. This is the frame in which the moments are applied and rotations are measured.

For the analysis, the helicopter rotor is modeled as a spinning disc with a diameter of 24 cm, a thickness of 1.5 mm and a mass of 3.35 grams. The rotational frequency is 60 Hz. The differential equations are solved for an applied moment $M_x = 1$ mNm in the non-spinning reference frame. Figure 6-5 show the resulting rotational accelerations, velocities and positions of the system. Figure 6-5a shows that the accelerations about the x- and y-axis both average to zero. The average of the rotational velocities (Figure 6-5b) is not zero around the y-axis, due to the phase difference in acceleration. This is an interesting fact: An applied moment around the x-axis results in a rotational velocity around the y-axis. This is called gyroscopic precession. The effect is often described as a 90° phase shift of the applied moment in the direction of spin, but that is actually incorrect.

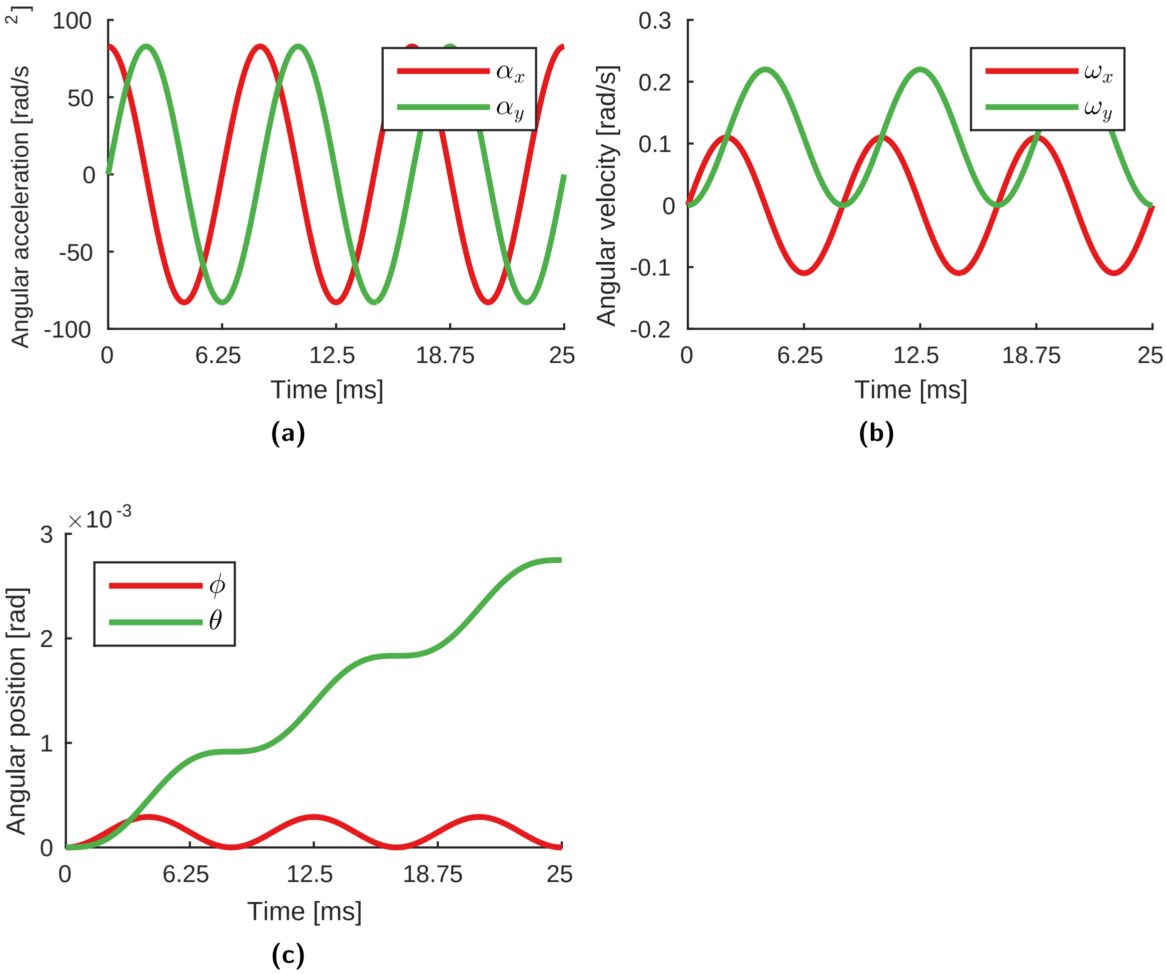

Figure 6-5: Time response of a spinning disc to an applied moment $M_x = 1$mNm. The disc spins at 60 Hz and has a diameter of 24 cm, a thickness of 1.5 mm and a mass of 3.35

6-4 Control

There are no research projects with similar size helicopters. Control theories for larger helicopters can still be applicable and are investigated in this section.

6-4-1 PID control

PID is a common type of controller used for attitude stabilization of helicopters. ArduPilot is an autopilot platform which has code specifically designed for helicopters. It consists of three separate PID controllers for the angular rates. There is also a feed-forward term in each rate control loop. This term adds a control deflection that scales the requested angular rate. The feed-forward term is added because a non-zero control deflection is required for a sustained angular velocity. Attitude stabilization is done with simple P controllers. The angular errors are inputs and commanded angular rates are the outputs of the stabilization controllers.

This method of control does not account for cross-couplings. If the collective is increased, the torque on the helicopter increases because of aerodynamic drag. The tail-rotor pitch has to be increased to compensate for this. With the PID controller as described here, this compensation is accomplished by the yaw rate controller. Large gains minimize the deflection of the tail.

Increasing the thrust of the tail rotor also causes a sideways acceleration. This can only be compensated by tilting the rotor disc. This is not included in the PID controllers. Eventually, the position control loop will compensate for sideways drift.

PID control is a popular control method for hobbyists. There are a few research projects on autonomous helicopters that use PID control as well Mejas et al. (2006); Saripalli et al. (2003).

6-4-2 Other control methods

Although PID is the most common type of controller, a wide range of control methodologies have been used for helicopters. These methodologies include input/output linearization Koo & Sastry (1998), gain scheduling Sprague et al. (2001), LQR control Gavrilets et al. (2001); Jiang et al. (2006), neural networks Johnson et al. (2003); Leitner et al. (1995) and reinforcement learning Schölkopf et al. (2007). INDI control has not yet been attempted on helicopters and will be discussed in the next chapter.

Chapter 7

Incremental Nonlinear Dynamic Inversion for Helicopter Control

The idea to use INDI for helicopter control originates from Simplicio et al. (2013). Section 7-1 describes the motivation to choose this type of controller for a helicopter. Sections 7-2 and 7-3 describe the mathematics of Nonlinear Dynamic Inversion (NDI) and INDI. Section 7-4 describes a proposed new method on how a rigid spinning disc, which is a greatly simplified model of a helicopter, can be controlled using INDI.

7-1 Motivation

Helicopters are very complex and non-linear systems. The desire for a flight control system is to provide good maneuverability while assuring stability. The flight controller should also be robust, meaning that it should continue to work reliably in case of a inaccuracies. Such inaccuracies could arise from different sources. Examples of inaccuracies are shifts in center of gravity, or different battery sizes and weights.

Adaptive control systems are able to identify and update parameters of a model online. The model is then inverted and used to calculate control inputs, as for example in NDI. However, it is difficult to guarantee that the adaptive algorithm will never learn incorrectly. Also, it is hard to show that the system will be able recover from failures in adaption Simplicio et al. (2013).

INDI is a nonlinear control method which calculates incremental control inputs instead of the total inputs. The incremental input is based on feedback from acceleration measurements. Thereby the controller continues to increment the control inputs as long as there is a mismatch between the desired and actual accelerations. With this control strategy, only the relations between control inputs and acceleration measurements are required. Even when the system is not affine in control inputs, the Jacobian matrix can be used as demonstrated by Simplicio et al. (2013). The part of the model which depends only on the system states is not needed.

This makes it automatically more robust against model mismatch, since the model is not used.

In Simplicio et al. (2013), these benefits of an INDI controller are demonstrated for a full scale helicopter in a simulation study. The current research project is aimed at implementing the INDI control strategy for a small scale model helicopter.

7-2 Nonlinear Dynamic Inversion

NDI is a technique developed in the 1970s for control of nonlinear systems. It is applicable to the class of systems that are feedback linearizable Slotine & Li (1991). The relations between the virtual control inputs and the outputs of the system are reduced to simple integrators. These integrators can be controlled with a simple linear controller. In a Multiple Input Multiple Output (MIMO) system, the controlled dimensions are completely decoupled.

The basic principles of NDI and INDI are explained by Simplicio et al. (2013). The description that follows is based on that explanation. A general system to which NDI can be applied is described by:

$$\begin{aligned}\dot{\mathbf{x}} &= \mathbf{f}(\mathbf{x}) + \mathbf{G}(\mathbf{x})\mathbf{u} \\ \mathbf{y} &= \mathbf{h}(\mathbf{x})\end{aligned} \tag{7-1}$$

where $\mathbf{f}$ and $\mathbf{h}$ are vectors in $\mathbb{R}^n$ and $\mathbb{R}^m$ respectively and $\mathbf{G}$ is the n x m control effectiveness matrix.

The general NDI procedure is to differentiate $\mathbf{y}$ until the input vector $\mathbf{u}$ appears explicitly in the equation. By choosing $\mathbf{h}(\mathbf{x}) = \mathbf{x}$, the input vector appears explicitly after the first differentiation:

$$\dot{\mathbf{y}} = \dot{\mathbf{x}} = \mathbf{f}(\mathbf{x}) + \mathbf{G}(\mathbf{x})\mathbf{u} \tag{7-2}$$

A virtual control input ν can be chosen as $\nu = \dot{\mathbf{x}}$ if $\det \mathbf{G}(\mathbf{x}) \neq 0$. The INDI loop will then regulate the output $\dot{\mathbf{x}}$ to the virtual control. The virtual control is set by a simple linear controller. The required control input to the system is then given by:

$$\mathbf{u} = \mathbf{G}^{-1}(\mathbf{x})\left[\nu - \mathbf{f}(\mathbf{x})\right] \tag{7-3}$$

An accurate description of $\mathbf{f}$ and $\mathbf{G}$ is required to cancel all the nonlinearities and cross-couplings in the system. If the system has uncertainties, exact cancellation of nonlinearities is impossible. This is demonstrated by adding uncertainties in the equation:

$$\dot{\mathbf{x}} = \mathbf{f}_n(\mathbf{x}) + \Delta\mathbf{f}(\mathbf{x}) + (\mathbf{G}_n(\mathbf{x}) + \Delta\mathbf{G}(\mathbf{x}))\mathbf{u} \tag{7-4}$$

The subscript n indicates the nominal parts known to the controller. When $\mathbf{u}$ is substituted by Eq. 7-3 with only the nominal part ($\mathbf{G} = \mathbf{G}_n$), the relation $\nu = \dot{\mathbf{x}}$ is only retrieved if the uncertain parts are zero:

$$\dot{\mathbf{x}} = \Delta\mathbf{f}(\mathbf{x}) - \Delta\mathbf{G}(\mathbf{x})\mathbf{G}_n^{-1}(\mathbf{x})\mathbf{f}_n(\mathbf{x}) + (\mathbf{I}_{n\times n} + \Delta\mathbf{G}(\mathbf{x})\mathbf{G}_n^{-1}(\mathbf{x}))\nu \tag{7-5}$$

Adaptive NDI is one way to handle uncertainties. Parameters in the model $\mathbf{f}$ and actuator effectiveness matrix $\mathbf{G}$ are identified online. Because of the online identification, the model becomes an accurate description of the system and the uncertain parts are reduced.

7-3 Incremental Nonlinear Dynamic Inversion

The problem with uncertainties in the system can also be solved with Incremental NDI (INDI). Instead of calculating the control inputs $\mathbf{u}$, the increments in control inputs $\Delta\mathbf{u}$ are calculated. A linear approximation of the system is obtained by a first-order Taylor series expansion of Eq. 7-2 at each instant in time:

$$\dot{\mathbf{x}} \approx \dot{\mathbf{x}}_0 + \frac{\partial}{\partial \mathbf{x}} \left[\mathbf{f}(\mathbf{x}) + \mathbf{G}(\mathbf{x})\mathbf{u}\right]_{\mathbf{x}_0,\mathbf{u}_0} (\mathbf{x} - \mathbf{x}_0) + \mathbf{G}(\mathbf{x}_0)(\mathbf{u} - \mathbf{u}_0) \tag{7-6}$$

When assuming that $\mathbf{u}$ can change significantly faster than $\mathbf{x}$ and if the controller has a high sampling frequency, it can also be assumed that $\mathbf{x} \approx \mathbf{x}_0$. In that case, Eq. 7-6 can be reduced to

$$\dot{\mathbf{x}} \approx \dot{\mathbf{x}}_0 + \mathbf{G}(\mathbf{x}_0)(\mathbf{u} - \mathbf{u}_0) \tag{7-7}$$

The control law to achieve $\nu = \dot{\mathbf{x}}$ is then given by

$$\mathbf{u} = \mathbf{G}^{-1}(\mathbf{x}_0)(\nu - \dot{\mathbf{x}}_0) + \mathbf{u}_0 \tag{7-8}$$

where $\mathbf{x}_0$ is obtained by sensor measurements. That is why this approach is sometimes referred to as sensor based control, as opposed to model based control. The applied control input $\mathbf{u}_0$ needs to be known accurately. Uncertainties in the model are no longer present, but there can still be uncertainties in the control effectiveness matrix $\mathbf{G}$. Eq. 7-7 then turns into

$$\dot{\mathbf{x}} = \dot{\mathbf{x}}_0 + (\mathbf{G}_n(\mathbf{x}_0) + \Delta\mathbf{G}(\mathbf{x}_0))(\mathbf{u} - \mathbf{u}_0) \tag{7-9}$$

Applying the control law of Eq. 7-8 with $\mathbf{G}(\mathbf{x}_0) = \mathbf{G}_n(\mathbf{x}_0)$ then yields

$$\dot{\mathbf{x}} = \dot{\mathbf{x}}_0 + (\mathbf{G}_n(\mathbf{x}_0) + \Delta\mathbf{G}(\mathbf{x}_0))\mathbf{G}_n^{-1}(\mathbf{x}_0)(\nu - \dot{\mathbf{x}}_0) \tag{7-10}$$

which can be further reduced to:

$$\dot{\mathbf{x}} = \dot{\mathbf{x}}_0 + (\nu - \dot{\mathbf{x}}_0) + \Delta\mathbf{G}(\mathbf{x}_0)\mathbf{G}_n^{-1}(\mathbf{x}_0)(\nu - \dot{\mathbf{x}}_0) \tag{7-11}$$

$$\dot{\mathbf{x}} = \nu + \Delta\mathbf{G}(\mathbf{x}_0)\mathbf{G}_n^{-1}(\mathbf{x}_0)(\nu - \dot{\mathbf{x}}_0) \tag{7-12}$$

This means that the relation $\dot{\mathbf{x}} = \nu$ is only obtained if $\Delta\mathbf{G}(\mathbf{x}_0) = \mathbf{0}$.

7-3-1 Actuator dynamics

In real systems, it is usually not possible to make immediate changes in the control input $\mathbf{u}$. With the actuator dynamics captured in $\mathbf{A}(z)$, the INDI control scheme is provided in Figure 7-1. The inner part that constructs the control input $\mathbf{u}$ from a desired differential input $\Delta\mathbf{u}_c$ has the following discrete transfer function:

$$\frac{\mathbf{u}}{\Delta\mathbf{u}_c} = \frac{\mathbf{A}(z)}{1 - \mathbf{A}(z)z^{-1}} \tag{7-13}$$

The complete system dynamics can be derived from Figure 7-1:

$$\dot{\mathbf{x}} = (\nu - \dot{\mathbf{x}}z^{-1})\mathbf{G}^{-1}\frac{\mathbf{A}(z)}{1 - \mathbf{A}(z)z^{-1}}\mathbf{G} \tag{7-14}$$

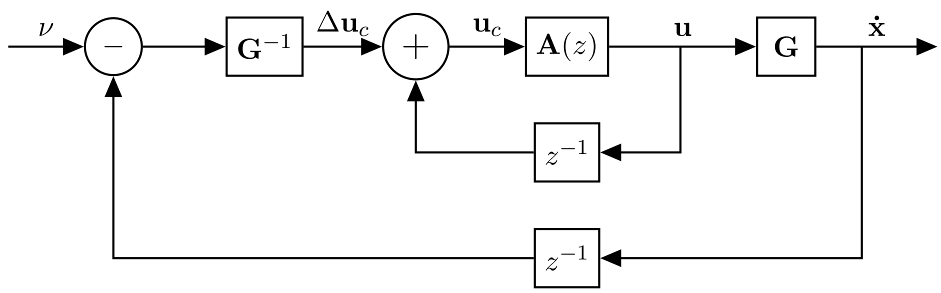

Figure 7-1: INDI control scheme with actuator dynamics.

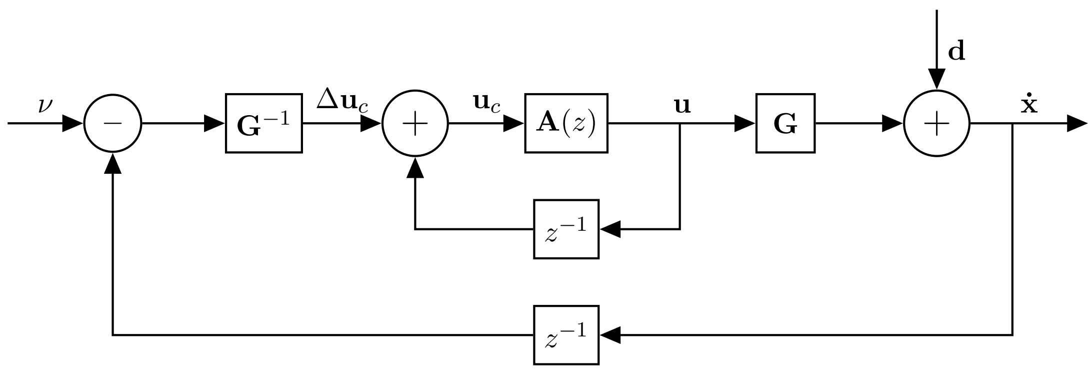

Figure 7-2: INDI control scheme with actuator dynamics and external disturbance.

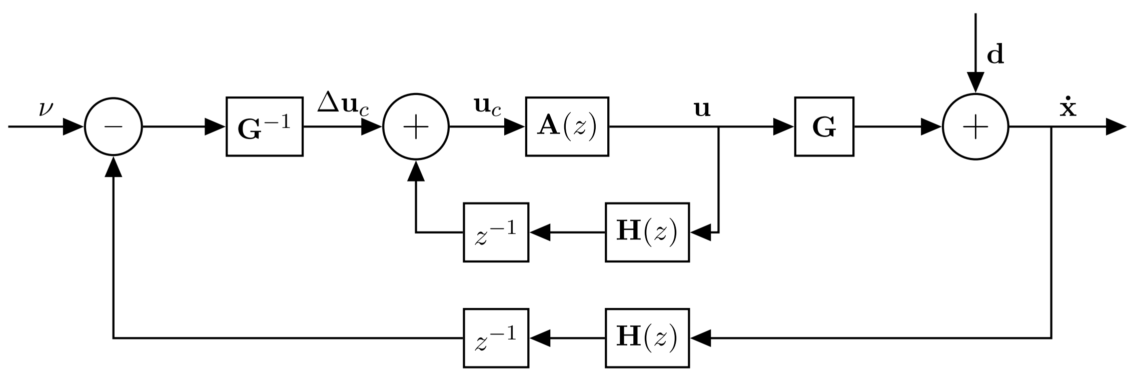

Figure 7-3: INDI control scheme with actuator dynamics, external disturbance and measurement filter.

Only if the actuator dynamics are equal for each actuator, such that $\mathbf{A}(z) = \mathbf{I}_{n\times n}a(z)$, the terms $\mathbf{G}^{-1}$ and $\mathbf{G}$ cancel each other. Eq. 7-14 can then be reduced as follows:

$$\dot{\mathbf{x}} = (\nu - \dot{\mathbf{x}}z^{-1})\frac{\mathbf{A}(z)}{1-\mathbf{A}(z)z^{-1}} \tag{7-15}$$

$$\left[1 + \frac{\mathbf{A}(z)z^{-1}}{1-\mathbf{A}(z)z^{-1}}\right]\dot{\mathbf{x}} = \frac{\mathbf{A}(z)}{1-\mathbf{A}(z)z^{-1}}\nu \tag{7-16}$$

Now multiplying both sides with $(1 - \mathbf{A}(z)z^{-1})$ gives:

$$\left[\left(1 - \mathbf{A}(z)z^{-1}\right) + \mathbf{A}(z)z^{-1}\right]\dot{\mathbf{x}} = \dot{\mathbf{x}} = \nu\mathbf{A}(z) \tag{7-17}$$

This shows that the system will be as fast as the actuator dynamics. If the actuators do not have the same dynamics, the control signals of the faster actuators can be filtered to give an equal response. As mentioned in Section 7-3, the actual position of the actuators needs to be known precisely. Depending on the type of actuator, it might be possible to measure the actual output. If this is not possible, an accurate model of the actuator dynamics is required.

7-3-2 Disturbance rejection

Real systems will also be subject to external disturbances. An important aspect of the controller is the ability to reject disturbances. The output of the system due to disturbances can be derived from Figure 7-2 as

$$\dot{\mathbf{x}}_d = \mathbf{d} - \frac{\mathbf{A}(z)\cdot z^{-1}}{1-z^{-1}\mathbf{A}(z)}\dot{\mathbf{x}}_d \tag{7-18}$$

$$\dot{\mathbf{x}}_d\left(1 + \frac{z^{-1}\mathbf{A}(z)}{1-z^{-1}\mathbf{A}(z)}\right) = \mathbf{d} \tag{7-19}$$

$$\frac{\dot{\mathbf{x}}_d}{\mathbf{d}} = \frac{1}{\left(1+\frac{z^{-1}\mathbf{A}(z)}{1-z^{-1}\mathbf{A}(z)}\right)} = \frac{1}{\left(1+\frac{\mathbf{A}(z)}{z-\mathbf{A}(z)}\right)}\cdot\frac{z-\mathbf{A}(z)}{z-\mathbf{A}(z)} = \frac{z-\mathbf{A}(z)}{z} = 1 - \frac{\mathbf{A}(z)}{z} \tag{7-20}$$

This equation shows that disturbance rejection depends on the actuator dynamics. The faster the actuator dynamics, the faster it rejects disturbances to the system.

7-3-3 Output measurement filtering

The described INDI approach assumes perfect sensors to measure $\mathbf{x}_0$. Real sensors are not perfect but may produce noisy data. Especially when differentiating rate measurements to obtain accelerations Smeur et al. (2015). It is undesirable that the controller responds to measurement noise. If the measurement data is filtered with for example a low-pass filter, there is no longer a direct input-output relation. The INDI controller will add more control input until the filtered measurement shows the desired output. This will cause an overshoot and can make the entire system unstable. The knowledge that the measurement data is filtered must be included in the construction of the control input signal.

If the same filter is also included in the construction of the input signal as in Figure 7-3, the transfer function of the complete system will be exactly the same as Eq. 7-17. However, the performance in disturbance rejection is affected. Using a similar derivation as for Eq. 7-20, it can be shown that the effect of disturbances to the output is given by

$$\frac{\dot{\mathbf{x}}_d}{\mathbf{d}} = 1 - \frac{\mathbf{A}(z)\mathbf{H}(z)}{z} \tag{7-21}$$

The slower the output measurement filter $\mathbf{H}(z)$ is, the slower disturbances are rejected as well.

7-4 INDI for helicopter rate control

Since the rigid body dynamics of a spinning disc are comparable to the dynamics of a spinning helicopter rotor, it is interesting to study how such a system can be controlled with INDI. Traditionally, the angular rates of the UAV are chosen in the state vector $\mathbf{x}$ Simplicio et al. (2013); Smeur et al. (2015), so that the first derivative describes the angular accelerations. This makes perfect sense for multi-rotors, since the revolutions per minute (RPM) of the motors are directly proportional to the resultant angular accelerations. Therefore, the control effectiveness matrix contains constant numbers. For helicopters however, the control effectiveness then becomes a complex set of equations which is not affine in the control inputs. A Jacobian matrix of the control effectiveness functions replaces the control effectiveness matrix. Because of its complexity, this has to be done numerically Simplicio et al. (2013).

7-4-1 Incremental rate control loop

A simpler method is proposed here. The control inputs for a helicopter are swash plate position and orientation. By varying the swash plate orientation, an aerodynamic moment is generated by the rotor blades. Section 6-3 shows that applied moments on a spinning disc are proportional to an average angular velocity in the perpendicular axis. A hingeless helicopter is simulated by adding a body to this disc with a spring-damper link. The roll rate of the body then behaves as a low-pass filter to control input, just as in Figure 6-3 and as in Eq. 6-2. The roll rate response of an arbitrary hingeless helicopter is modeled as:

$$H(s) = \frac{\dot{\phi}(s)}{\theta_{lat}(s)} = \frac{g_{\dot{\phi}}}{1 + \frac{s}{\omega_c}} \tag{7-22}$$

where $\dot{\phi}$ is the roll rate, θ_{lat} is the cyclic input for roll, $g_{\dot{\phi}}$ is the steady state roll rate and ω_c is the bandwidth. The steady-state roll rate is directly proportional with the cyclic input. Although this is a heavily simplified model, it shows that no affine relation exists between roll rate and control input. The equation does not fit in the form of Eq. 7-1.

The new method uses the steady state value $g_{\dot{\phi}}$ as control effectiveness, while the dynamics are handled as actuator dynamics. Figure 7-4 shows the control scheme for incremental roll rate control. The virtual control ν is the roll rate reference $\dot{\phi}_{ref}$. If there are no disturbances, the system will respond exactly as the open loop system given in Eq. 7-22. The transfer function is derived as follows:

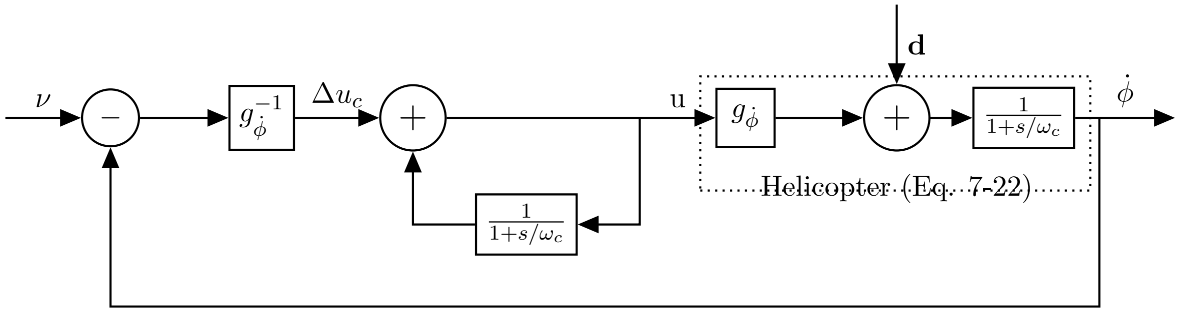

Figure 7-4: INDI control scheme for roll rate control.

$$\frac{u(s)}{\Delta u_c(s)} = \frac{1}{1 - \frac{1}{1+s/\omega_c}} = \frac{1+s/\omega_c}{1+s/\omega_c - 1} = \frac{1+s/\omega_c}{s/\omega_c} \tag{7-23}$$

$$H_{OL}(s) = g_{\dot\phi}^{-1} \frac{u}{\Delta u_c} g_{\dot\phi} \frac{1}{1+s/\omega_c} = \frac{1+s/\omega_c}{s/\omega_c} \frac{1}{1+s/\omega_c} = \frac{\omega_c}{s} \tag{7-24}$$

$$\frac{\dot\phi(s)}{\nu(s)} = \frac{H_{OL}(s)}{1+H_{OL}(s)} = \frac{\omega_c/s}{1+\omega_c/s} = \frac{\omega_c}{s+\omega_c} = \frac{1}{1+s/\omega_c} \tag{7-25}$$

This shows that the response is exactly the same as in Eq. 7-22. However, the system of Eq. 7-22 is not able to reject disturbances, while the control scheme of Figure 7-4 is. The transfer function which describes the effect of disturbance on the roll rate is derived as follows:

$$\frac{\dot\phi(s)}{d(s)} = \frac{\frac{1}{1+s/\omega_c}}{1+H_{OL}(s)} = \frac{\frac{1}{1+s/\omega_c}}{1+\omega_c/s} = \frac{1}{(1+s/\omega_c)(1+\omega_c/s)} \tag{7-26}$$

$$\frac{\dot\phi(s)}{d(s)} = \frac{1}{1+s/\omega_c+\omega_c/s+1} = \frac{s}{s^2/\omega_c+2s+\omega_c} = \frac{\omega_c s}{s^2+2\omega_c s+\omega_c^2} \tag{7-27}$$

The transfer function describes a critically damped second order system. It is also possible to make the system faster by multiplying Δu_c with a gain $K_{\Delta u}$. Using a similar derivation as for Eqs. 7-25 and 7-27, it can be shown that the transfer functions of the system become:

$$\frac{\dot\phi(s)}{\nu(s)} = \frac{1}{1+\frac{s}{K_{\Delta u}\omega_c}} \tag{7-28}$$

$$\frac{\dot\phi(s)}{d(s)} = \frac{\omega_c s}{s^2+(K_{\Delta u}+1)\omega_c s+K_{\Delta u}\omega_c^2} \tag{7-29}$$

This shows that by increasing the gain $K_{\Delta u}$, the helicopter responds quicker to control inputs and disturbances.

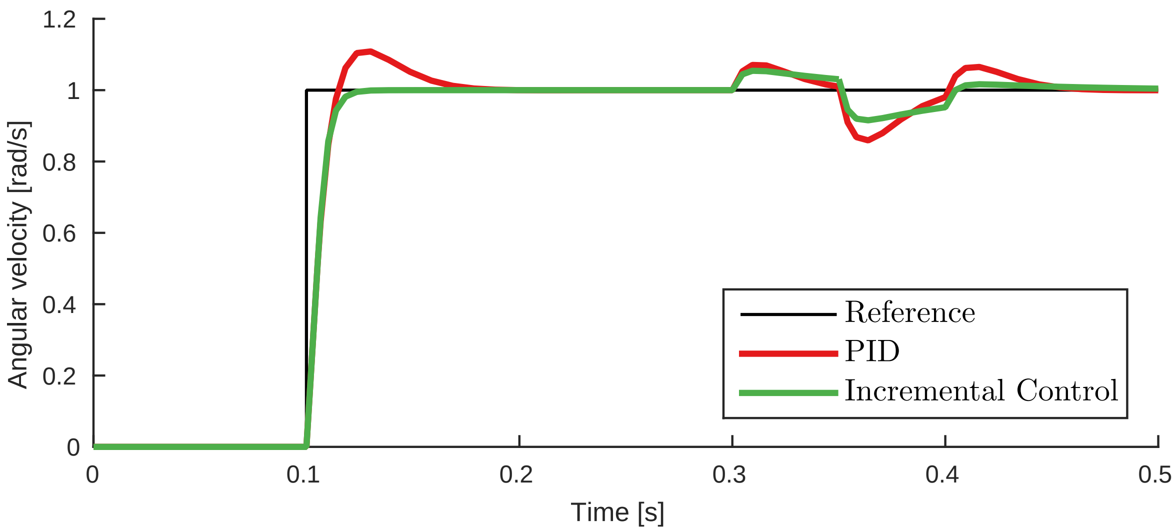

(a) Roll rate.

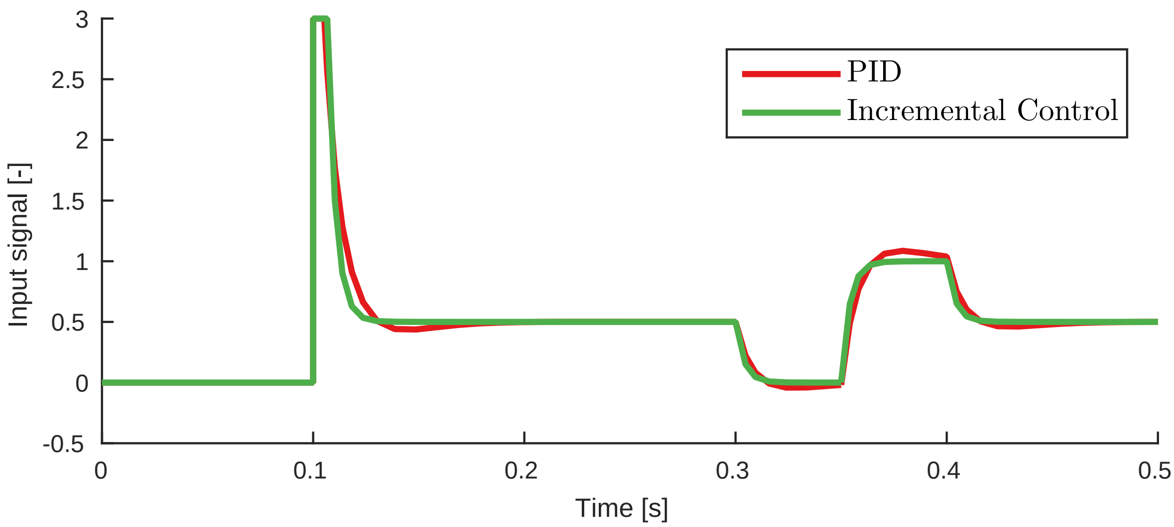

(b) Control inputs with saturation.

Figure 7-5: Helicopter roll rate and control input in response to a step input and a doublet disturbance with a PID controller and an incremental controller.

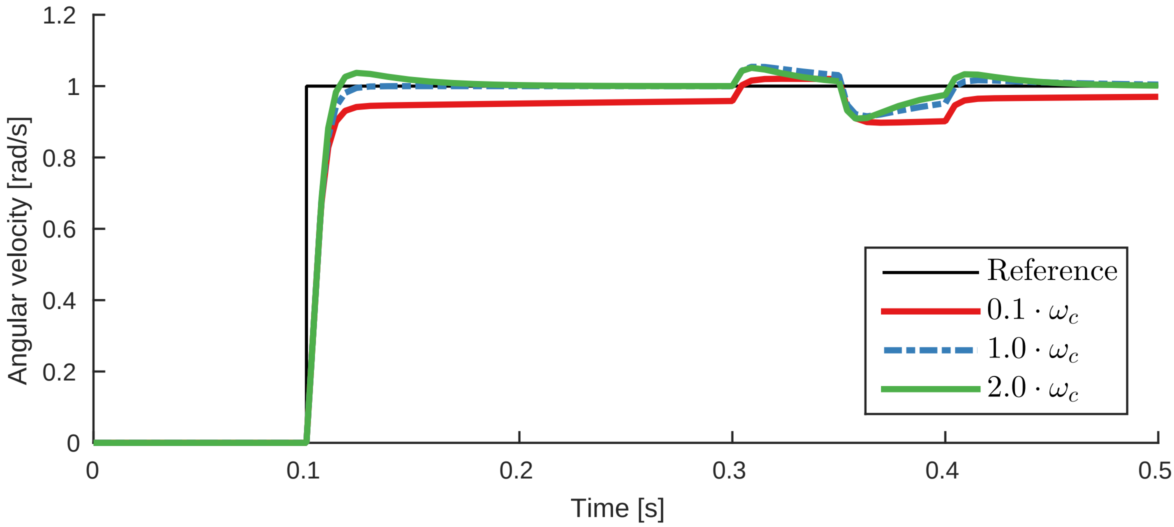

Figure 7-6: Roll rate response to a step input and a doublet disturbance with different values for ω_c in the feedback model. $K_{\Delta u}$ is 15 in all three cases.

7-4-2 Simulation

A simulation study is performed to see how the controller responds to control inputs and disturbances. The response of a simple PID controller is given as a reference. It is not fair to compare the controllers in a pure theoretical study. The gain $K_{\Delta u}$ can be increased to very large numbers which will result in an almost perfect response.

In the simulation, a saturation level applies to the control inputs. A step input is commanded as reference roll rate. A gain $K_{\Delta u}$ of 15 is used. The roll rate in Figure 7-5a shows no overshoot because the system is first order (see Eq. 7-28). Between 0.3 and 0.4 seconds, a doublet disturbance signal is fed into the system. The incremental controller responds to the disturbance according to Eq. 7-29.

The response of the incremental controller is defined by the steady state control effectiveness $g_{\dot{\phi}}$ and the first order model in the incremental feedback loop. If these are not accurately modeled, the helicopter should still stabilize towards the requested roll rate. Inaccuracy in $g_{\dot{\phi}}$ will have the same effect as $K_{\Delta u}$: it will make the response and disturbance rejection faster or slower.

If the first order model in the incremental feedback loop has a higher bandwidth ω_c than the actual helicopter, the input signal u will be higher. That will result in overshoot, but is quickly compensated. If the bandwidth in the in the model is lower than in the actual helicopter, the control input u will be lower and the roll rate will stabilize at a lower value than the reference. The difference is then slowly compensated so that it eventually reaches the reference value. Figure 7-6 shows the response for correctly and wrongly estimated values of the actual bandwidth ω_c.

The simulation study shows that the control concept works in theory, but it is only for pitch and roll. Integration with yaw and vertical motion is left for the main phase of the project.

Chapter 8

Project Planning

The goal of the project is to make the helicopter fly autonomously outside using INDI. The remainder of the project can be divided in two parts: attitude estimation and implementation of an INDI controller. The second part can only be started with if the attitude estimation works. Figure 8-1 shows a global planning of next project phases.

8-1 Attitude estimation

Two categories of attitude estimation algorithms are studied in Chapter 5. The Kalman filter shows the best performance in literature. A complementary filter has also been applied successfully numerous times in literature. The advantage of the complementary filter is that it requires less computational power for results that are close to those of a Kalman filter. A complementary filter is preferred because of the limited processing power on the Lisa/S autopilot.

The paparazzi autopilot project already has a quaternion implementation of a complementary filter which can be used. This can be extended with a set of notch filters to remove the strongest vibrations from the accelerometer signals. It is also important to implement a proper method of threshold switching, to make the complementary filter temporarily ignore accelerometer measurements when dynamic accelerations are detected.

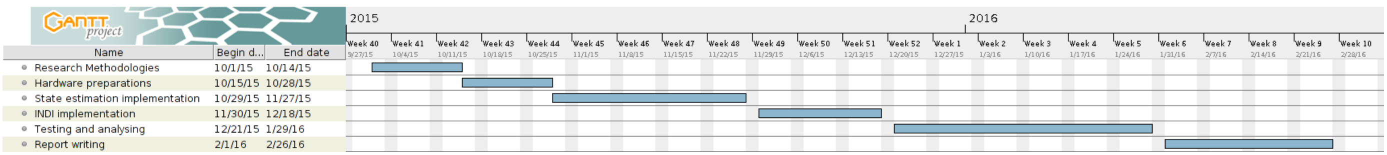

Figure 8-1: Gantt chart of the global project planning.

The performance of the attitude estimation algorithm can be analyzed in the OptiTrack arena. The helicopter can use standard PID control for these flights. If the results are satisfying, the project continues to the next phase.

8-2 INDI controller implementation

The incremental control method which is proposed for control of rotational rates works in theory. Some test flights need to be done using a standard PID controller to identify the helicopter control dynamics. If these test results show that the roll rate can be modeled as a first order system, the incremental control method can be implemented. Otherwise, the method from Simplicio et al. (2013) can be implemented.

Once the INDI controller is implemented, it can be tested in the OptiTrack arena to analyze its performance. If the helicopter can fly autonomously in the arena without problems, the same can be tried outside using GPS. Then, the goal of the project is achieved and everything will be written down in a final thesis.

Chapter 9

Conclusions

Just like for the research questions, the conclusions are divided in two sections. The first is related to attitude estimation while the second section is about INDI control of a helicopter.

9-1 Attitude estimation

MEMS gyroscopes and acceleromters are the most common type found on UAVs. They are very small, light-weight and cheap. Integration of MEMS gyroscope measurements drifts very quickly. Accelerometers are used to compensate drift. The two most commonly used attitude estimation algorithms to fuse these measurements are Kalman filters and complementary filters. Kalman filters perform slightly better, but require more computational power. A complementary filter is chosen since the processing power of the processor on the Lisa/S is limited.

Accelerometers do not only measure gravity, but also dynamic accelerations and vibrations. Dynamic accelerations can be dealt with using threshold switching, which makes the estimation process rely only on the gyroscopes for a short period of time. Vibrations can be filtered with notch filters which are centered at the main rotor frequency and its first harmonics.

9-2 Helicopter INDI control

Three main categories of helicopter rotors are teetering, articulated and hingeless. The model helicopter used in this project has a hingeless rotor. For this type of helicopter, the body responds quickly to control inputs.

INDI has already been applied successfully on quadcopters. A theoretical study exists for helicopters, but this implementation has complicated control effectiveness functions. A simpler method is proposed in which the relation between roll rate and control input is modeled as a first order system. The steady state value of the first order system describes the control effectiveness, while the dynamics are handled as actuator dynamics. If the real helicopter shows a similar relation between control inputs and angular velocities, this method can be applied in practice. This method is designed only for pitch and roll. The combination with control of yaw and vertical motion will be investigated in the main phase of the project.

Bibliography

Baerveldt, A. J., & Klang, R. (1997a, Sep). A low-cost and low-weight attitude estimation system for an autonomous helicopter. In *Intelligent engineering systems, 1997. ines '97. proceedings., 1997 ieee international conference on* (p. 391-395).

Baerveldt, A. J., & Klang, R. (1997b, Sep). A low-cost and low-weight attitude estimation system for an autonomous helicopter. In *Intelligent engineering systems, 1997. ines '97. proceedings., 1997 ieee international conference on* (p. 391-395).

Barshan, B., & Durrant-Whyte, H. F. (1995, Jun). Inertial navigation systems for mobile robots. *Robotics and Automation, IEEE Transactions on*, *11*(3), 328-342.

Bijker, J., & Steyn, W. (2008). Kalman filter configurations for a low-cost loosely integrated inertial navigation system on an airship. *Control Engineering Practice*, *16*(12), 1509 - 1518.

Bing, Z., Qiang, W., Zewei, Z., & Wei, H. (2012, July). Control testbed design for a miniature autonomous helicopter. In *Control conference (ccc), 2012 31st chinese* (p. 4383-4388).

Bramwell, A., Done, G., & Balmford, D. (2000). 5 - flight dynamics and control. In A. Bramwell, G. Done, & D. Balmford (Eds.), *Bramwell's helicopter dynamics* (Second Edition ed., p. 137 - 195). Oxford: Butterworth-Heinemann.

Brown, R. G., & Hwang, P. Y. C. (1992). *Introduction to random signals and applied kalman filtering*. New York: J. Wiley.

Carminati, M., Ferrari, G., Grassetti, R., & Sampietro, M. (2012, Oct). Real-time data fusion and mems sensors fault detection in an aircraft emergency attitude unit based on kalman filtering. *Sensors Journal, IEEE*, *12*(10), 2984-2992.

Choukroun, D., Bar-Itzhack, I., & Oshman, Y. (2006, Jan). Novel quaternion kalman filter. *Aerospace and Electronic Systems, IEEE Transactions on*, *42*(1), 174-190.

Driessens, S., & Pounds, P. E. I. (2013, Nov). Towards a more efficient quadrotor configuration. In *Intelligent robots and systems (iros), 2013 ieee/rsj international conference on* (p. 1386-1392).

Euston, M., Coote, P., Mahony, R., Kim, J., & Hamel, T. (2008, Sept). A complementary filter for attitude estimation of a fixed-wing uav. In *Intelligent robots and systems, 2008. iros 2008. ieee/rsj international conference on* (p. 340-345).

Fennelly, J., Ding, S., Newton, J., & Zhao, Y. (2012, Mar). Thermal mems accelerometers fit many applications.

Foxlin, E. (1996, Mar). Inertial head-tracker sensor fusion by a complementary separate-bias kalman filter. In *Virtual reality annual international symposium, 1996., proceedings of the ieee 1996* (pp. 185-194, 267).

Gavrilets, V., Shterenberg, A., Martinos, I., Sprague, K., Dahleh, M., & Feron, E. (2001, Sep). Avionics system for aggressive maneuvers. *Aerospace and Electronic Systems Magazine, IEEE*, *16*(9), 38-43.

Gebre-Egziabher, D., Hayward, R., & Powell, J. D. (2004, April). Design of multi-sensor attitude determination systems. *Aerospace and Electronic Systems, IEEE Transactions on*, *40*(2), 627-649.

Gebre-Egziabher, D., Hayward, R. C., & Powell, J. D. (1998, Apr). A low-cost gps/inertial attitude heading reference system (ahrs) for general aviation applications. In *Position location and navigation symposium, ieee 1998* (p. 518-525).

Greene, M. E., & Trent, V. (2003). Software algorithms in air data attitude heading reference systems. *Aircraft Engineering and Aerospace Technology*, *75*(5), 470-476.

Hamel, T., & Mahony, R. (2006, May). Attitude estimation on so[3] based on direct inertial measurements. In *Robotics and automation, 2006. icra 2006. proceedings 2006 ieee international conference on* (p. 2170-2175).

Higgins, W. T. (1975, May). A comparison of complementary and kalman filtering. *Aerospace and Electronic Systems, IEEE Transactions on*, *AES-11*(3), 321-325.

Jensen, A., Coopmans, C., & Chen, Y. (2013, May). Basics and guidelines of complementary filters for small uas navigation. In *Unmanned aircraft systems (icuas), 2013 international conference on* (p. 500-507).

Jiang, Z., Han, J., Wang, Y., & Song, Q. (2006, Jan). Enhanced lqr control for unmanned helicopter in hover. In *Systems and control in aerospace and astronautics, 2006. isscaa 2006. 1st international symposium on* (p. 6 pp.-1443).

Johnson, E., , Johnson, E. N., & Schrage, D. P. (2003). The georgia tech unmanned aerial research vehicle: Gtmax. In *in proceedings of the aiaa guidance, navigation, and control conference* (pp. 2003–5741).

Kang, C. W., & Park, C. G. (2009, Aug). Attitude estimation with accelerometers and gyros using fuzzy tuned kalman filter. In *Control conference (ecc), 2009 european* (p. 3713-3718).

Kim, A., & Golnaraghi, M. F. (2004, April). A quaternion-based orientation estimation algorithm using an inertial measurement unit. In *Position location and navigation symposium, 2004. plans 2004* (p. 268-272).

Kim, C., Kim, T., & Lyou, J. (2012, Oct). Realization of a mems attitude reference system for a small aerial vehicle. In *Iecon 2012 - 38th annual conference on ieee industrial electronics society* (p. 1567-1570).

Kim, H. J., Jordan, M. I., Sastry, S., & Andrew, Y. (2004). Autonomous helicopter flight via reinforcement learning. In S. Thrun, L. Saul, & B. Schölkopf (Eds.), *Advances in neural information processing systems 16* (pp. 799–806). MIT Press.

Koo, T., & Sastry, S. (1998, Dec). Output tracking control design of a helicopter model based on approximate linearization. In *Decision and control, 1998. proceedings of the 37th ieee conference on* (Vol. 4, p. 3635-3640 vol.4).

Leavitt, J., Sideris, A., & Bobrow, J. E. (2006, June). High bandwidth tilt measurement using low-cost sensors. *Mechatronics, IEEE/ASME Transactions on*, *11*(3), 320-327.

Lee, J. K., & Park, E. J. (2009, May). A minimum-order kalman filter for ambulatory real-time human body orientation tracking. In *Robotics and automation, 2009. icra '09. ieee international conference on* (p. 3565-3570).

Lee, J. K., Park, E. J., & Robinovitch, S. N. (2012, Aug). Estimation of attitude and external acceleration using inertial sensor measurement during various dynamic conditions. *Instrumentation and Measurement, IEEE Transactions on*, *61*(8), 2262-2273.

Leitner, J., Calise, A., & Prasad, J. (1995). *Analysis of adaptive neural networks for helicopter flight controls.*

Li, W., & Wang, J. (2013, 1). Effective adaptive kalman filter for mems-imu/magnetometers integrated attitude and heading reference systems. *The Journal of Navigation*, *66*, 99–113.

Lundberg, M., Nordlund, P. J., & Stahl-Gunnarsson, K. (2000). Synthetic attitude and heading reference for saab gripen. In *Decision and control, 2000. proceedings of the 39th ieee conference on* (Vol. 3, p. 2040-2043 vol.3).

Mahony, R., Hamel, T., & Pflimlin, J.-M. (2005, Dec). Complementary filter design on the special orthogonal group so(3). In *Decision and control, 2005 and 2005 european control conference. cdc-ecc '05. 44th ieee conference on* (p. 1477-1484).

Mahony, R., Hamel, T., & Pflimlin, J.-M. (2008, June). Nonlinear complementary filters on the special orthogonal group. *Automatic Control, IEEE Transactions on*, *53*(5), 1203-1218.

Makni, A., Fourati, H., & Kibangou, A. Y. (2014, June). Adaptive kalman filter for mems-imu based attitude estimation under external acceleration and parsimonious use of gyroscopes. In *Control conference (ecc), 2014 european* (p. 1379-1384).

Martin, H., Groves, P. D., Newman, M., & Faragher, R. (2013, Sep). A new approach to better low-cost mems imu performance using sensor arrays. In *Proceedings of the 26th international technical meeting of the satellite division of the institute of navigation* (p. 2125-2142).

Mejas, L., Saripalli, S., Campoy, P., & Sukhatme, G. S. (2006). Visual servoing of an autonomous helicopter in urban areas using feature tracking. *Journal of Field Robotics*, *23*.

Padfield, G. D. (2008). Modelling helicopter flight dynamics: Building a simulation model. In *Helicopter flight dynamics* (p. 93). Blackwell Publishing Ltd.

Rehbinder, H., & Hu, X. (2001). Drift-free attitude estimation for accelerated rigid bodies. In *Robotics and automation, 2001. proceedings 2001 icra. ieee international conference on* (Vol. 4, p. 4244-4249 vol.4).

Remes, B. D. W., Esden-Tempski, P., Van Tienen, F., Smeur, E., De Wagter, C., & De Croon, G. C. H. E. (2014, Aug). Lisa-s 2.8g autopilot for gps-based flight of mavs. *Proceedings 2014 IMAV*, 280-285.

Roberts, J. M., Corke, P. I., & Buskey, G. (2003, Sept). Low-cost flight control system for a small autonomous helicopter. In *Robotics and automation, 2003. proceedings. icra '03. ieee international conference on* (Vol. 1, p. 546-551 vol.1).

Sabatini, A. M. (2006, July). Quaternion-based extended kalman filter for determining orientation by inertial and magnetic sensing. *Biomedical Engineering, IEEE Transactions on*, *53*(7), 1346-1356.

Saripalli, S., Roberts, J., Corke, P., Buskey, G., & Sukhatme, G. (2003, Oct). A tale of two helicopters. In *Intelligent robots and systems, 2003. (iros 2003). proceedings. 2003 ieee/rsj international conference on* (Vol. 1, p. 805-810 vol.1).

Schölkopf, B., Platt, J., & Hofmann, T. (2007). An application of reinforcement learning to aerobatic helicopter flight. In *Advances in neural information processing systems 19:proceedings of the 2006 conference* (p. 1-8). MIT Press.

Setoodeh, P., Khayatian, A., & Frajah, E. (2004, 5). Attitude estimation by separate-bias kalman filter-based data fusion. *The Journal of Navigation*, *57*, 261-273.

Simplicio, P., Pavel, M. D., van Kampen, E., & Chu, Q. P. (2013). An acceleration measurements-based approach for helicopter nonlinear flight control using incremental nonlinear dynamic inversion. *Control Engineering Practice*, *21*(8), 1065-1077.

Slotine, J.-J. E., & Li, W. (1991). Applied nonlinear control. *NJ: Prantice-Hall, Englewood Cliffs*.

Smeur, E., Chu, Q., & de Croon, G. (2015). Adaptive nonlinear dynamic inversion for attitude control of micro aerial vehicles. *Journal of Guidance, Control and Dynamics [submitted]*.

Son, Y., Shin, H., Kim, D., Park, Y., Noh, J., Choi, K., et al. (2015, August). Rocking drones with intentional sound noise on gyroscopic sensors. In *24th usenix security symposium (usenix security 15)* (pp. 881–896). Washington, D.C.: USENIX Association.

Sprague, K., Gavrilets, V., Dugail, D., Mettler, B., Feron, E., & Martinos, I. (2001, Oct). Design and applications of an avionics system for a miniature acrobatic helicopter. In *Digital avionics systems, 2001. dasc. 20th conference* (Vol. 1, p. 3C5/1-3C5/10 vol.1).

Suh, Y. S. (2006, June). Attitude estimation by multiple-mode kalman filters. *Industrial Electronics, IEEE Transactions on*, *53*(4), 1386-1389.

Suh, Y. S. (2010, Dec). Orientation estimation using a quaternion-based indirect kalman filter with adaptive estimation of external acceleration. *Instrumentation and Measurement, IEEE Transactions on*, *59*(12), 3296-3305.

Suh, Y. S., Park, S. K., Kang, H. J., & Ro, Y. S. (2006). Attitude Estimation Adaptively Compensating External Acceleration. *JSME International Journal Series C*, *49*, 172-179.

Vaganay, J., Aldon, M. J., & Fournier, A. (1993, May). Mobile robot attitude estimation by fusion of inertial data. In *Robotics and automation, 1993. proceedings., 1993 ieee international conference on* (p. 277-282 vol.1).

Wang, M., Yang, Y., Hatch, R. R., & Zhang, Y. (2004, April). Adaptive filter for a miniature mems based attitude and heading reference system. In *Position location and navigation symposium, 2004. plans 2004* (p. 193-200).

Won, S. h. P., Golnaraghi, F., & Melek, W. W. (2009, May). A fastening tool tracking system using an imu and a position sensor with kalman filters and a fuzzy expert system. *Industrial Electronics, IEEE Transactions on*, *56*(5), 1782-1792.

Won, S. H. P., Melek, W. W., & Golnaraghi, F. (2010, May). A kalman/particle filter-based position and orientation estimation method using a position sensor/inertial measurement unit hybrid system. *Industrial Electronics, IEEE Transactions on*, *57*(5), 1787-1798.

Xiong, K., Liang, T., & Yongjun, L. (2011). Multiple model kalman filter for attitude determination of precision pointing spacecraft. *Acta Astronautica*, *68*(78), 843 - 852.

Yun, X., Lizarraga, M., Bachmann, E. R., & McGhee, R. B. (2003, Oct). An improved quaternion-based kalman filter for real-time tracking of rigid body orientation. In *Intelligent robots and systems, 2003. (iros 2003). proceedings. 2003 ieee/rsj international conference on* (Vol. 2, p. 1074-1079 vol.2).